高度医療技術開発室

室長　是恒之宏

室員　安部晴彦

近年における医療を取り巻く情報処理や画像処理の技術革新により、診断、治療における医用画像診断装置の利用範囲は拡大しており、著しいイノベーションを引き起こしています。医用画像診断装置の技術開発により低侵襲化、従来視覚化困難であった部位や現象の画像化が可能になりつつあり、そこから新たな治療が生まれる可能性があります。これらの技術開発には医工連携すなわち病院、大学、企業との連携体制の構築が必要ですが、米国における産学連携の仕組みや組織と比較すると本邦ではまだまだ発展の余地が多いと言えるでしょう。本研究室では病院における医療現場のニーズを、企業が保有している技術開発力や大学の基礎医学研究能力に結び付けながら、常に新しい高度医療技術（特に医用画像診断装置）の開発に取り組んでいきます。

現在、当研究室の主要な課題は、コントラスト剤を用いた心エコーによる心腔内血流イメージングです。心腔内のコントラストバブルを Particle Image Velocimetry (PIV 法) という画像解析手法を用いて心腔内血流を可視化しています。PIV 法は流体工学の分野で流体解析に用いられている手法であり、これを医用画像に応用することによって、心腔内血流動態というこれまで観察出来なかったものを観察することにより、心疾患の新たな病態解明の手段とすべく研究を行っています。

この新たな心エコーによる PIV 法を確立するためには動物実験が必要であり、大阪大学大学院医学系研究科保健学専攻機能診断科学講座の中谷敏教授とともに基礎研究を行っています。

【2013 年度研究発表業績】

A-0

Abe H, Caracciolo G, Kheradvar A, Pedrizzetti G, Khandheria BK, Narula J, Sengupta PP. Contrast echocardiography for assessing left ventricular vortex strength in heart failure: a prospective cohort study.　Eur Heart J - Cardiovascular Imaging. 2013;14(11):1049-60. (2013 年 4 月)

Caracciolo G, Goliasch G, Amaki M, Bansal M, Nakabo A, Abe H, Scott L, Lipar L, Pedrizzetti G, Narula J, Sengupta PP.　Myocardial stretch in early systole is a key determinant of the synchrony of left ventricular mechanical activity in vivo.Circ J. 2013;77(10):2526-34. (2013 年 7 月)

B-2

Abe H, Masuda K, Asanuma T, Koriyama H, Koretsune Y, Kusuoka H, Nakatani S. : Visualization of blood flow in the left ventricular short axis view by echocardiographic particle image velocimetry 35th Annual International Conference of the IEEE Engineering in Medicine and Biology Society, Osaka, Japan（2013 年 7 月）

B-4

安部晴彦、Sengupta P. Partho：コントラストエコーによる左室内渦流評価と左室機能に果たす役割。日本超音波医学会第 86 回学術集会、大阪（2013 年 5 月）

B-6

篠内和也、安部晴彦、廣岡慶治、古川哲生、坂口大起、三浦弘之、宮崎宏一、濱野剛、小出雅雄、安村良男、是恒之宏、楠岡英雄：医原性浅大腿仮性動脈瘤に対して超音波ガイド下トロンビン注入療法が有効であった 1 例。第 115 回日本循環器学会近畿地方会、京都（2013 年 6 月）

三浦弘之、安部晴彦、廣岡慶治、井上裕之、西田博毅、安村かおり、古川哲生、坂口大起、篠内和也、宮崎宏一、濱野剛、小出雅雄、北田博一、安村良男、是恒之宏、楠岡英雄：心エコーで観察できた雷撃症の一例。日本超音波医学会第 40 回関西地方会学術集会、大阪（2013 年 11 月）

井上裕之、安部晴彦、廣岡慶治、西田博毅、安村かおり、古川哲生、坂口大起、篠内和也、三浦弘之、宮崎宏一、濱野剛、小出雅雄、安村良男、是恒之宏、楠岡英雄：急性肺血栓塞栓症を発症した HIV 感染症患者の一例。第 116 回日本循環器学会近畿地方会、大阪（2013 年 11 月）

European Heart Journal – Cardiovascular Imaging (2013) **14**, 1049–1060
doi:10.1093/ehjci/jet049

Contrast echocardiography for assessing left ventricular vortex strength in heart failure: a prospective cohort study

Haruhiko Abe[1,2], Giuseppe Caracciolo[1,2], Arash Kheradvar[3], Gianni Pedrizzetti[2,4], Bijoy K. Khandheria[5], Jagat Narula[2], and Partho P. Sengupta[2]*

[1]Division of Cardiovascular Diseases, Mayo Clinic, Scottsdale, AZ, USA; [2]Zena and Michael A. Wiener Cardiovascular Institute, Mount Sinai School of Medicine, One Gustave L. Levy Place, PO Box 1030, New York, NY 10029, USA; [3]Department of Biomedical Engineering, University of California, Irvine, CA, USA; [4]Dipartimento Ingegneria e Architettura, University of Trieste, Italy; and [5]Aurora Sinai/Aurora St Luke's Medical Centers, University of Wisconsin School of Medicine and Public Health, Milwaukee, WI, USA

Received 28 December 2012; accepted after revision 12 March 2013; online publish-ahead-of-print 14 April 2013

Aims This study investigated the incremental role of echocardiographic-contrast particle image velocimetry (Echo-PIV) in patients with heart failure (HF) for measuring changes in left ventricular (LV) vortex strength (VS) during phases of a cardiac cycle.

Methods and results Echo-PIV was performed in 42 patients, including 23 HF patients and 19 controls. VS was measured as a fluid-dynamic parameter that integrates blood flow rotation over a given area and correlated with non-invasively derived indices of LV mechanical performance. In comparison with early and late diastole, the VS was higher during isovolumic contraction (IC) for control and HF patients with the preserved ejection fraction ($P = 0.002$ and $P = 0.01$, respectively), but not for HF patients with the reduced ejection fraction ($P = 0.41$). On multivariable regression analysis, the VS during IC (VS_{IC}) was independently related to late-diastolic VS and LV longitudinal strain ($R^2 = 0.63$, $P < 0.001$ and $P = 0.003$, respectively). Patients in whom diastolic VS was augmented during IC showed a higher LV stroke volume ($P = 0.01$), stroke work ($P = 0.02$), and mechanical efficiency ($P = 0.008$). Over a median follow-up period of 2.9 years, eight (34%) HF patients were hospitalized for decompensated HF. In comparison with the rest, these eight patients showed markedly reduced longitudinal strain ($P = 0.002$), and lower change in VS ($P = 0.004$).

Conclusion Our preliminary data suggest that the persistence of vortex from late diastole into IC is a haemodynamic measure of coupling between diastole and systole. The change in VS is correlated with LV mechanical performance and shows association with adverse clinical outcomes seen in HF patients.

Keywords Particle image velocimetry • Vortex • Left ventricle • Mechanical efficiency • Heart failure

Introduction

Several numerical models, *in vitro* experiments, and imaging studies have shown that the transmitral blood flow during early-diastolic filling results in the formation of a left ventricular (LV) intracavitary vortex.[1–8] The LV vortex has been suggested to minimize kinetic energy dissipation and reduces the total energy required for eventual ejection.[1–8] Preliminary observations have further suggested that LV remodelling results in attenuation of the blood flow kinetic energy.[9] Given the complexity and the number of assumptions involved in experimental studies and relative dearth of data in humans, confirmation of proposed flow dynamics with the direct measurement of the blood flow sequence in clinical settings is crucial.

Kilner *et al.*[10] suggested that diastolic vortices are preserved by asymmetry of the flow paths that facilitate continued redirection of the blood flow towards the LV outflow for optimal ejection. Furthermore, the vortex formed in diastole persists into the period of isovolumic contraction (IC), which follows the mitral valve closure and is characterized by a rapid rise in LV pressure

* Corresponding author: The Mount Sinai Medical Center, One Gustave L. Levy Place, PO Box 1030, New York, New York 10029. Tel: +1 212 659 9121; Fax: +1 212 849 2674. Email: partho.sengupta@mountsinai.org

before opening of the aortic valve.[11] An organized LV intracavitary blood flow into IC may enhance coupling between diastole and systole, optimizing LV performance; however, the relationship of the LV flow to wall mechanics is a topic that has not been directly validated in clinical settings.

Echocardiographic-contrast particle image velocimetry (Echo-PIV) allows flow quantification;[12] its concept has been approve for vascular measurements and validated in accurate *in vitro* settings.[12–14] The feasibility of Echo-PIV for visualizing the LV flow has been recently validated[15,16] and potential applications have been verified in experimental[11] and clinical settings.[16] For the present investigation, we hypothesized that the strength of vortex persisting from diastolic filling into IC is a haemodynamic marker, that is, associated with LV mechanical performance. The present investigation, therefore, explored the spatial and temporal characteristics of the two-dimensional (2D) blood flow in relation to LV mechanical activity in compensated heart failure (HF) patients attending outpatient clinic (ACC/AHA Stage C or D HF).[17] Vortex strength (VS) was quantified as the total rotation rate of the flow in a bounded region. Asymptomatic patients with risk factors who were found to have normal LV structure and function on screening echocardiograms (ACC/AHA Stage A)[17] were used as a non-HF control group.

Methods

We identified 47 consecutive subjects including 27 consecutive patients with Stage C or D compensated HF and 20 asymptomatic patients with risk factors who underwent an outpatient echocardiogram between July 2008 and July 2010 with a single provider (P.S.). The subjects were subsequently consented for an additional contrast echocardiogram. Exclusion criteria included decompensated HF, LV aneurysm, inotropic support at the time of evaluation, atrial fibrillation, hypertrophic or restrictive cardiomyopathy, pericardial diseases, valve disease (valvular stenosis or more than mild valvular regurgitation), primary pulmonary hypertension, congenital heart disease, acute coronary event or coronary artery bypass graft surgery (within 3 months), pregnancy, and patient refusal/inability to sign the informed consent form. Of the 47 patients, 5 were excluded because of suboptimal 2D or contrast echocardiographic image quality. Of the remaining 42 patients, 23 belonged to Stage C or D compensated HF with 10 patients having preserved ejection fraction (HFPEF) and 13 patients having the reduced ejection fraction (HFREF; $<$50%). Demographic features, risk factors, New York Heart Association class, and treatment are shown in *Table 1*. The institutional review board approved the study and all patients provided written informed consent.

Standard B-mode and Doppler echocardiography

Cine loops from three standard apical views (four-chamber, two-chamber, and apical long-axis) and short-axis views at the mitral valve, papillary and apical levels were recorded using greyscale harmonic imaging (Vivid 7, GE Medical Systems, Horten, Norway), following the guidelines recommended by the American Society of Echocardiography.[18] End-diastolic and end-systolic volumes were used to calculate the ejection fraction by Simpson's biplane method from the apical four- and two-chamber views. Pulsed-wave Doppler echocardiography was performed to obtain early and late-diastolic transmitral flow velocities. Pulsed-wave tissue Doppler velocities were measured at the septal and lateral mitral annulus in the four-chamber view and were averaged for obtaining mean early-diastolic mitral annulus velocity and the ratio of early-diastolic transmitral flow velocity to early-diastolic mitral annulus velocity. Diastolic dysfunction and its severity was described as per the published recommendations.[19] We also calculated LV sphericity index,[20] LV stroke work,[21] and LV mechanical efficiency (ratio of stroke work/myocardial oxygen consumption, simplified as the amount of blood pumped by a single heart beat in 1 s.[22–25]), as per previously determined definitions.

Speckle-tracking strain echocardiography

LV subendocardial longitudinal and circumferential strain and radial strain from full thickness of the myocardium were measured (50–80 frames/s) using the 2D Cardiac Performance Analysis© software (TomTec Imaging Systems, Munich, Germany), an extended version of a previously validated software (*syngo*® Velocity Vector Imaging™, Siemens Medical Solutions USA, Inc., Malvern, PA, USA).[26] Net LV twist was calculated as the net difference between LV peak rotation angles obtained from basal (CW, clockwise) and apical (CCW, counterclockwise) short-axis planes. Dyssynchrony was measured as the standard deviation of the time to minimum (for longitudinal and circumferential) or to maximum (for radial) strain obtained from 16 LV segments.

Contrast echocardiography

Two-dimensional contrast echocardiography was performed with a perfluoropropane gas-filled, lipid-stabilized microbubble (Definity®, Lantheus Medical Imaging, Inc., North Billerica, MA, USA; 0.1–0.2 mL infused intravenously as bolus injection). Two-dimensional images of the intraventricular flow were obtained from the apical long-axis view at a mechanical index of 0.1–0.4. The width and depth of the ultrasound scan area (*Figure 1*) and the spatial temporal settings were optimized to achieve the highest possible frame rates (204 $\pm$ 39 frames/s).

Images were acquired when the bubble density and motion were optimal and best visually appreciable. On the one hand, the density of bubble had to be sufficient to appreciate their individual motion, on the other, saturation had to be avoided to make bubbles distinguishable. To verify this, we first obtained anatomical M-mode images from the 2D contrast scans along the central scanning axis as described previously (*Figure 2*).[11] This acquisition ensures that the same bubbles remain in the scan plane for finite period of time resulting into the formation of streaks in the dark blood pool. The presence of these streaks ensures that the bubble density is optimal for creating speckle patterns that can be tracked in the ultrasonic scan plane. Nevertheless, it was previously demonstrated theoretically[27] that the bubble density has only a weak influence on the results of image analysis for blood motion.

Echocardiographic particle image velocimetry

Echo-PIV uses pairs of sequential digital images for calculating the direction and magnitude of the fluid flow.[12,14,16] For this, contrast images with particles were exported into files as a stack of images during a cardiac cycle and were analysed frame by frame with a PIV software (time-resolved analysis, INSIGHT™ 3G TSI, Inc., Shoreview, MN, USA[11]) to obtain the velocity vector field (*Figure 1*). The interrogation window of 32 $\times$ 64 pixels with 50% overlap was used for analysis. Maximal particle displacement was $<$16 pixels in *x*-axis direction and $<$32 pixels in *y*-axis direction during the first interrogation and adjusted until optimal Echo-PIV tracking was achieved. The reliability of the evaluated velocities that may be affected by either local

Table 1. Baseline characteristics of study subjects

	Non-HF control (n = 19)	Heart failure		P-value
		HFPEF (n = 10)	HFREF (n = 13)	
Age (years)	61 ± 10	65 ± 12	75 ± 7*,***	0.001
Female gender (%)	8 (42)	3 (30)	1 (7)	0.10
Body surface area (m^2)	1.88 ± 0.28	1.87 ± 0.20	1.98 ± 0.19	0.37
Systolic blood pressure (mmHg)	132 ± 17	129 ± 19	135 ± 22	0.80
Diastolic blood pressure (mmHg)	77 ± 10	70 ± 15	73 ± 10	0.21
Heart rate (beats/min)	67 ± 11	72 ± 19	72 ± 13	0.71
PR (ms)	156 ± 17	132 ± 30	142 ± 38	0.05
QRS (ms)	88 ± 10	117 ± 29**	167 ± 40*,***	<0.001
QRS >120 ms (%)	1 (5)	4 (40)	11 (84)	<0.001
Left bundle branch block (%)	1 (5)	0 (0)	3 (23)	0.15
NYHA class	—	1.3 ± 0.6	2.1 ± 0.9	0.02
Risk factors (%)				
Diabetes	2 (10)	3 (30)	5 (38)	0.16
Hypertension	10 (52)	4 (40)	9 (69)	0.36
Hyperlipidaemia	8 (42)	4 (40)	11 (84)	0.03
Coronary artery disease	2 (10)	1 (10)	8 (61)	0.002
Renal failure(Cr >1.2)	0 (0)	6 (60)	5 (38)	0.37
Medications (%)				
ACEI or ARB	1 (5)	3 (30)	10 (76)	<0.001
Beta blocker	4 (21)	7 (70)	11 (84)	<0.001
Calcium-channel blocker	2 (10)	3 (30)	1 (7)	0.25
Digoxin	—	—	4 (30)	—
Diuretics	2 (10)	8 (80)	8 (61)	<0.001

EF, ejection fraction; HFPEF, HF with preserved EF; HFREF, HF with the reduced ejection fraction; NYHA, New York Heart Association; ACEI, angiotensin-converting enzyme inhibitor; ARB, angiotensin receptor blocker.
*$P < 0.05$ non-HF control vs. HFREF.
**$P < 0.05$ non-HF control vs. HFPEF.
***$P < 0.05$ HFPEF vs. HFREF.

absence or contrary excessive saturation of contrast agent is automatically monitored by the software by excluding vectors with small cross-correlation coefficient. To find subpixel displacement, we used a three-point, two-direction, Gaussian peak fitting in one dimension Illustrative figures and movies were prepared using the dedicated software (Hyperflow, Amid.net, Sulmona, Italy).

Once the velocity field was obtained, the spatial distribution of *vorticity* was computed, at every frame, using Tecplot (Tecplot, Inc., Bellevue, Washington, DC, USA). Vorticity, which corresponds to the local angular velocity of a fluid particle, represents the key quantity in fluid dynamics as it permits the delineation and quantification of vortices and shear layers. Mathematically, it is computed by taking the curl of velocity vector. Vorticity (i, j, t) was calculated by numerical derivatives.

$$\text{Vorticity} = 1000 \times \left\{ \frac{Vy(i+1,j) - Vy(i-1,j)}{x(i+1,j) - x(i-1,j)} - \frac{Vx(i,j+1) - Vx(i,j-1)}{y(i,j+1) - y(i,j-1)} \right\}$$
$$= 1000 \times \left(\frac{dVy}{dx} - \frac{dVx}{dy} \right).$$

Units are as follows: x (mm), y (mm), Vx (m/s), and Vy (m/s).

Vorticity is a useful quantity to describe the underlying structure of a moving fluid. A region with compact vorticity represents a region with circular streamlines and constitutes a vortex; a region with elongated vorticity distribution exhibits a difference of velocity between the two sides and, thus, constitutes a shear layer, which serves as a boundary layer in vicinity of the wall. A brief introduction of the role vorticity for the cardiac flow has been recently reviewed[28]; and a more in-depth discussion on the same topic can be found elsewhere.[29]

In integral terms, vorticity defines the amount of circulatory (swirling) fluid dynamics. To evaluate such a feature of the motion, vorticity distribution was plotted in the form of a histogram based on the percentage of the map area vs. the vorticity values ω (s^{-1}) throughout the entire flow map (*Figure 3*). Based on conventions, CCW and CW vorticity are represented in red and blue, respectively, on the contour map.

Following the procedure outlined in *Figure 3*, we further characterized the amount of CW and CCW swirl by the circulation, that is, computed by taking the product of the corresponding mean vorticity and the area occupied by such vorticity within the area enclosed by the scanned image boundary. VS refers to the total amount of swirl (or circulation), and was calculated by summing up the value of the both the CW and the CCW values of the circulation. Early and late diastole and IC periods were delineated as previously described[11] and average VS was calculated during each of these three periods.

VS_{IC} was considered augmented if the magnitude was greater than the VS attained during early or late diastole (VS_E or VS_A). We also calculated the absolute change in VS from early diastole to IC and expressed it as a fractional change in VS from early diastole to IC ($[VS_{IC} - VS_E]/VS_{IC}$).

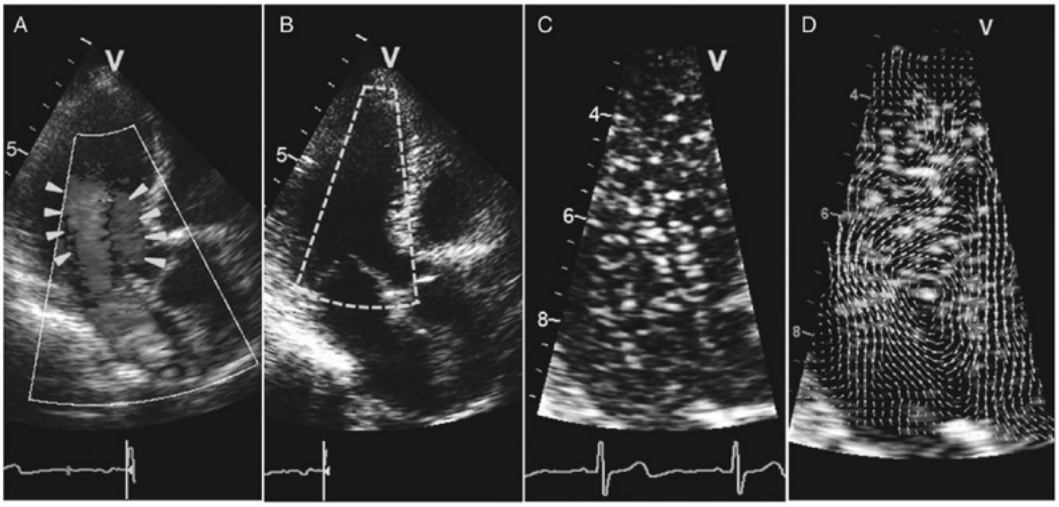

Figure 1. Echocardiographic-contrast particle imaging velocimetry. (*A*) Colour Doppler imaging showing the bidirectional flow during early diastole. (*B*) Delineation of the region of interest in the submitral and LV outflow region. (*C*) High-temporal resolution contrast echocardiography is performed for the region of interest. (*D*) Contrast particle imaging velocimetry shows the flow field with velocity vectors. Note the presence of a CW vortex (arrows).

Follow-up

Observed survival was assessed through a search of medical records and the Social Security Death Index on 1 November 2011. Rehospitalization for decompensated HF and all-cause mortality was recorded for each of the 23 HF patients from the date of echocardiography through November 2011, resulting in a median length of follow-up of 2.9 years. The following clinical events were reported as endpoints: cardiac death, hospitalization due to cardiac decompensation, or necessity for heart transplantation. The first event that occurred was used for the analysis.

Statistical analysis

Statistical analysis was performed with commercially available software (MedCalc 11.2, MedCalc Software, Mariakerke, Belgium). All continuous data were reported as means $\pm$ standard deviation, and categorical data as percentages. The Kruskal–Wallis test was used for non-parametric comparisons among independent non-HF control and HF groups and the Friedman test was used for non-parametric comparisons of repeated measurements of VS among cardiac cycle phases. The Mann–Whitney *U*-test was used for non--parametric comparisons of unpaired measurements between non-HF control and/or HF groups and the Wilcoxon rank-sum test was used for non-parametric comparisons of paired measurements of VS between cardiac cycle phases. The χ^2 test was used for comparisons of categorical variables. Univariate and multivariate linear regression analysis was performed to determine correlates of VS_{IC}. Statistical significance was defined as a two-tailed *P*-value <0.05. Intra-observer and inter-observer variability for the measurement of VS were calculated as means $\pm$ standard deviations of percentage ratios between absolute differences and means of the two independently measured variables in 10 randomly selected patients. Inter-observer agreement and intra-observer consistency were assessed with the Bland–Altman analysis.[30]

Results

Clinical characteristics

Differences in baseline clinical and echocardiographic characteristics for HF patients and non-HF controls are shown in *Tables 1* and *2*, respectively. HFREF patients were older ($P = 0.001$) with a higher prevalence of coronary artery disease ($P = 0.002$) and prolongation of QRS interval on surface electrocardiogram ($P < 0.001$). On echocardiography, HFREF patients showed significantly larger left atrial volume ($P = 0.004$), greater LV remodelling with the increased LV dimensions and sphericity index ($P < 0.001$ for each), and significantly increased ratio of the early-diastolic flow to mitral annular lengthening velocity ($P = 0.001$; *Table 2*). In comparison with non-HF controls and HFPEF, global LV strains in longitudinal, circumferential and radial directions, and net twist were significantly reduced in HFREF patients ($P < 0.05$ for each). Similarly, in comparison with non-HF controls and HFPEF, HFREF patients showed the presence of significant dyssynchrony in the longitudinal direction ($P = 0.01$).

LV fluid dynamics

For non-HF control, both VS_E and VS_A were similar in magnitude; however, the magnitude of VS_{IC} was significantly higher than VS_E and VS_A ($P = 0.01$ vs. and 0.002, respectively). Although VS_E in patients with HFPEF was lower than in non-HF controls ($P = 0.09$) and not different from VS_A, the magnitude of VS_{IC}

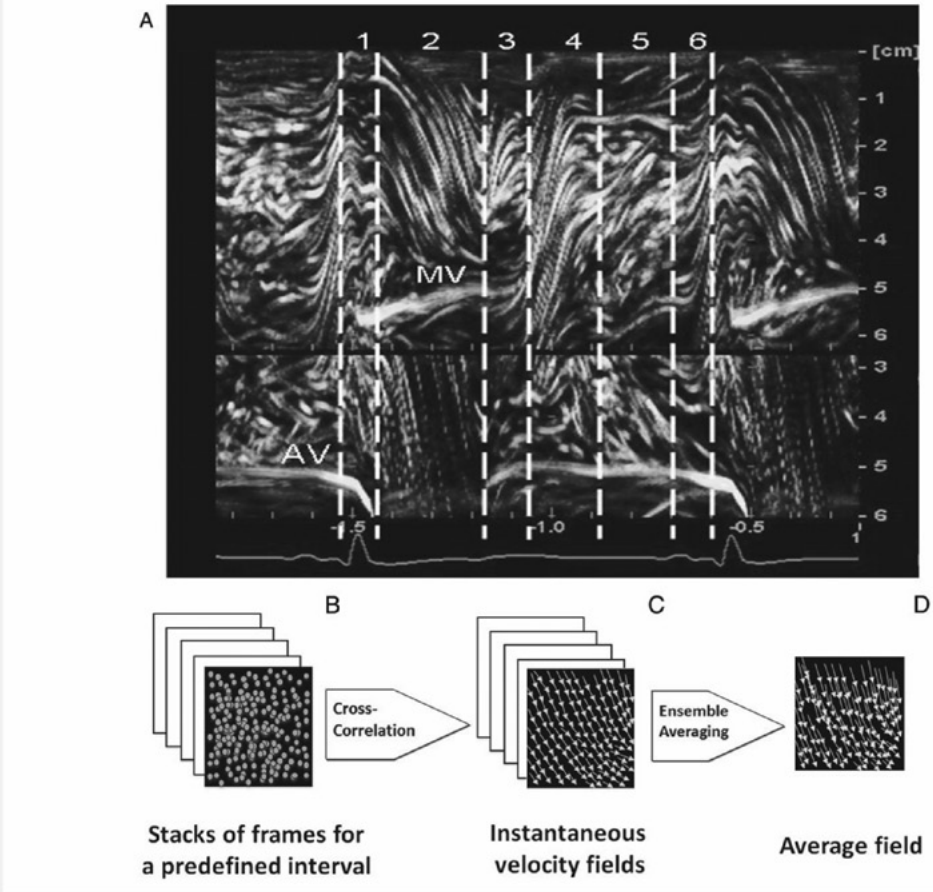

Figure 2. Assessment of LV intracavitary flow, contrast density, and motion. (*A*) An anatomical M-mode through the LV cavity during contrast infusion. The axial movement of contrast bubbles produces bright streaks, which suggest optimum contrast density and temporal resolution for tracking. The phases of cardiac cycle are then determined using the movement of the MV and the AV. Phases: 1, pre-ejection; 2, ejection; 3, isovolumic relaxation; 4, early diastole; 5, diastasis; and 6, late diastole. (*B*) Series of phase locked image frames are obtained during time intervals through the cardiac cycle as defined above. (*C*) Sequential pairs of these frames are cross-correlated for obtaining the velocity vectors. (*D*) Ensemble average of the sequential vector fields obtained for each time interval defines the dominant flow features in the flow field for that specific time interval.

was augmented and higher than VS_A ($P = 0.01$). In contrast, for patients with HFREF, VS_E was not significantly different than in non-HF controls, however, VS_{IC} failed to augment to a value higher than VS_E or VS_A (*Table 2* and *Figures 4* and *5*).

To understand the factors that contribute to VS_{IC}, we examined the univariate relationships between VS_{IC} and LV muscle and fluid mechanics variables (*Table 3*). On multivariable regression analysis, the magnitude of VS_{IC} was independently related to VS_E and LV longitudinal strain ($R^2 = 0.63$, $P < 0.001$). Similarly, the presence of dyssynchrony in the longitudinal strain was associated with VS_{IC} in HF patients ($r = -0.54$, $P = 0.04$). Supplementary data online, *Movies S1* and *S2* show a non-HF control subject with VS, that is, higher in IC, whereas Supplementary data online, *Movies S3* and *S4* illustrate an example of attenuated VS_{IC} in a patient with HFREF. The presence of greater VS_{IC} than the highest VS recorded during the diastolic phases was associated with a higher LV stroke volume (odds ratio: 1.09; confidence interval: 1.02–1.17; $P = 0.011$), stroke work (odds ratio: 1.03; confidence interval: 1.00–1.06; $P = 0.02$), and LV mechanical efficiency (odds ratio: 1.05; confidence interval: 1.01–1.10; $P = 0.008$). LV mechanical efficiency was related to longitudinal strain ($r = -0.38$, $P = 0.05$), radial strain ($r = 0.45$, $P = 0.005$), net LV twist ($r = 0.34$, $P = 0.02$), and VS change ($r = 0.38$, $P = 0.01$).

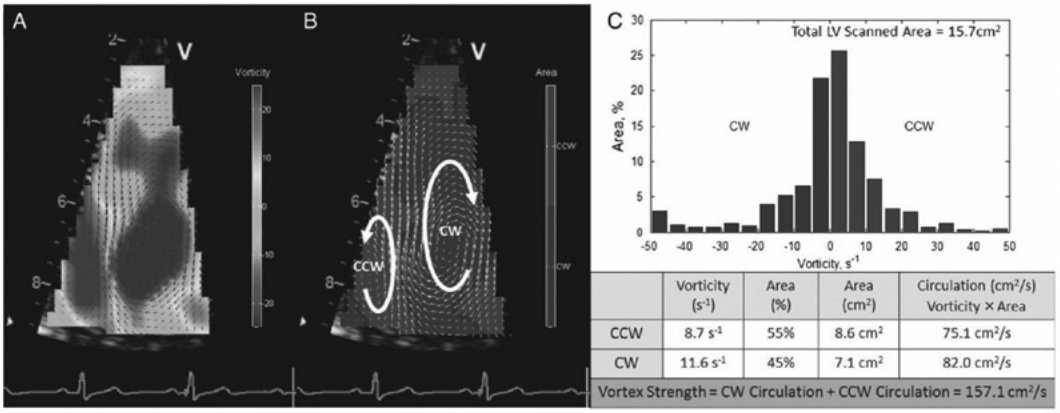

Figure 3. Calculation of circulation as a measure of VS. (*A*) Ensemble averaged vorticity distribution during early diastole. (*B*) Flow areas are separated into regions with CCW (red colour) and CW (blue colour) vorticity. (*C*) A histogram of CCW (positive vorticity) and CW (negative vorticity) is weighted by the percentage of area that takes such a value. Thus, the mean value of the positive and the negative vorticity is evaluated and the percentage of the corresponding areas is evaluated by summing up the histogram bins. The VS is computed by adding the circulation in CW and CCW directions (circulation is obtained by multiplying the mean vorticity with the corresponding areas).

Clinical follow-up and adverse events

Follow-up data were analysed in HF patients over a median follow-up period of 2.9 years. Of 23 patients, eight (34%) were hospitalized for decompensated HF, five (21%) patients died, and 1 patient underwent cardiac transplantation. Patients who reached an endpoint of death or hospitalization for HF ($n = 8$) showed a lower ejection fraction ($P = 0.08$) than remaining of the HF patients; however, had similar LA volumes and diastolic dysfunction. Patients with endpoints showed significantly lower longitudinal strain ($P = 0.002$), circumferential strain ($P = 0.04$), radial strain ($P = 0.02$), and lower change in VS ($P = 0.004$). The difference in VS change between the two groups persisted even after adjusting for the differences in LV EF ($P = 0.03$) (*Table 4*).

Inter-observer and intra-observer variability

The inter-observer and intra-observer variability for VS measurements were 7.7 ± 7.9 and 7.3 ± 7.8%, respectively. Bland–Altman analysis was used to assess inter-observer agreement and intra-observer consistency. Mean values, their differences, and the intraclass correlation coefficients are shown in Supplementary data online, *Table S1*. VS had good reproducibility with intraclass correlation coefficients ≥ 0.95 for most evaluations.

Discussion

This is the first prospective study that has (i) tested the phasic changes in the strength of intraventricular flow rotation (VS) in HF patients, using a fluid-dynamic variable computed through a high-temporal resolution Echo-PIV, which permits flow characterization during the phases of the cardiac cycle including the brief isovolumic phases, (ii) correlated the change in VS with non-invasively derived markers of LV systolic and diastolic performance including LV deformation and twist mechanics, and (iii) provided preliminary data regarding the change in VS from early diastole to IC in patients with HF with normal or reduced ejection fraction with further follow-up over a median period of 2.9 years for characterizing the potential prognostic value of change in VS.

VS during phases of cardiac cycle

A vortex develops in the form of a shear layer adjacent to the tissue (boundary layer). When the shear layer separates from the wall, fluid tends to curl into a vortex.[29] Previous investigations have studied the transmitral vortex formation using numerical or physical models or through flow visualization techniques such as cardiac magnetic resonance,[2,10,31–33] colour Doppler and contrast echocardiography.[11,16,34] The LV vortex characteristics in previous studies, however, have been primarily related to the diastolic filling phases of the cardiac cycle.[2–5,31,35] In an experimental model, we described the persistence of the LV vortex in early systole during the IC period; however, the relation between vortex during IC and LV mechanical activity was not previously assessed.[11] In a subsequent investigation, we also reported a close coupling of LV late-diastolic and IC mechanical activity and its utility in predicting peak oxygen consumption during exercise.[36] The present investigation further demonstrates the mechanical continuum of late-diastolic and IC phases of the cardiac cycle. A circulating blood flow during late diastole is smoothly continued into the phase of IC; where it becomes the eventual outcome of the diastolic vortex formation process that can relate with the LV mechanical activity

Table 2. Echocardiographic variables of study subjects

	Control (n = 19)	Heart failure		P-value
		HFPEF (n = 10)	HFREF (n = 13)	
Standard echocardiography				
LV septum (mm)	9 ± 1	11 ± 2	10 ± 2	0.11
LV posterior wall (mm)	9 ± 1	11 ± 2	10 ± 2	0.35
LV end-diastolic dimension (mm)	45 ± 6	44 ± 4	62 ± 7*,***	<0.001
LV end-systolic dimension (mm)	30 ± 4	29 ± 4	52 ± 9*,***	<0.001
LVEF (%)	63 ± 5	61 ± 7	28 ± 10*,***	<0.001
LV EDV (mL)	114 ± 40	113 ± 33	202 ± 79*,***	<0.001
LV ESV (mL)	41 ± 22	43 ± 17	146 ± 76*,***	<0.001
LVEF (%)	63 ± 5	61 ± 7	28 ± 10*,***	<0.001
Indexed LA volume (mL/m^2)	32 ± 9	43 ± 12**	48 ± 21*	0.004
E velocity (m/s)	0.74 ± 0.12	0.80 ± 0.29	0.80 ± 0.26	0.98
E/*A* ratio	1.1 ± 0.3	1.5 ± 0.6	1.7 ± 1.5	0.13
E/*e*′ mean	9.5 ± 3.1	13.3 ± 7.2**	22.5 ± 12.4*	0.001
Normal diastolic function (%)	14 (63)	—	—	—
Diastolic dysfunction (%)	5 (26)	10 (100)	13 (100)	<0.001
Grade I (%)	5 (26)	2 (20)	4 (31)	
Grade II (%)	—	7 (70)	4 (31)	
Grade III (%)	—	1 (10)	5 (38)	
RVSP (mmHg)	28 ± 5	39 ± 11**	42 ± 15*	0.007
LV sphericity index	0.54 ± 0.05	0.54 ± 0.05	0.65 ± 0.09*,***	<0.001
LV stroke volume (mL)	73 ± 19	70 ± 22	56 ± 14	0.08
LV stroke work (g)	119 ± 42	110 ± 43	90 ± 26	0.30
LV mechanical efficiency (mL/s)	69 ± 28	63 ± 26	49 ± 19	0.16
Strain, twist, and dyssynchrony				
Ls (%)	−18.3 ± 4.4	−15.2 ± 5.8	−9.8 ± 5.2*,***	<0.001
Cs (%)	−23.8 ± 4.6	−22.6 ± 7.4	−11.2 ± 6.1*,***	<0.001
Rs (%)	24.6 ± 9.6	19.7 ± 11.6	8.7 ± 5.2*,***	<0.001
Net twist (degree)	10.9 ± 5.6	11.7 ± 9.2	5.5 ± 3.6*	0.02
SD of time to Ls (ms)	50 ± 21	49 ± 23	81 ± 27*	0.01
SD of time to Cs (ms)	83 ± 31	69 ± 38	82 ± 40	0.61
SD of time to Rs (ms)	126 ± 47	116 ± 44	165 ± 63	0.17
Echocardiographic PIV				
VS_E (cm^2/s)	184 ± 57	143 ± 67	182 ± 67	0.19
VS_A (cm^2/s)	184 ± 67	143 ± 47	207 ± 118	0.15
VS_{IC} (cm^2/s)	231 ± 85****,*****	195 ± 103****,*****	203 ± 88	0.24
VS change	0.12 ± 0.33	0.21 ± 0.33	0.06 ± 0.24	0.37

LV, left ventricular; EF, ejection fraction; EDV, end-diastolic volume; ESV, end-systolic volume; LA, left atrium; E, early diastole; A, late diastole; *E*/*e*′, ratio of early-diastolic transmitral flow velocity to early-diastolic tissue velocity; RVSP, right ventricular systolic pressure; Ls, longitudinal strain; Cs, circumferential strain; Rs, radial strain; PIV, particle imaging velocimetry; VS_{IC}, vortex strength during isovolumic contraction; VS_E, vortex strength in early diastole; VS_A, vortex strength in late diastole; SD, standard deviation.
*$P < 0.05$ control vs. HFREF.
**$P < 0.05$ control vs. HFPEF.
***$P < 0.05$ HFPEF vs. HFREF.
****$P < 0.05$ VS_{IC} vs. VS_E.
*****$P < 0.05$ VS_{IC} vs. VS_A.

in systole. This suggests a potential role of IC vortex in optimizing diastolic-to-systolic mechanical coupling.

VS in HF

During the IC period, shortening of early activated regions of LV is accompanied with stretching of the late activated regions.[37,38] This reshaping deformation suggests interactions between the blood flow sequence and the LV mechanical activity developing in early systole.[39] Indeed, structural and functional remodelling of the LV results in an unfavourable mechanoenergetic profile (i.e. diminished mechanical efficiency)[40] and this change in mechanical efficiency may be related to the attenuation of the kinetic energy

of the diastolic LV flow.[9] Furthermore, a reduction in VS, during the IC period, may alter contractility of activated myocytes due to variations in preload that influence the steepness of the Frank–Starling relationship.[39] These novel insights, which link LV geometry, muscle, and fluid mechanics, raise several interesting hypotheses that require further verification.

Methodological considerations

The Echo-PIV technique has been previously validated in the laminar flow[41] and in the carotid bifurcation[14] with good agreement seen with optical particle imaging velocimetry for *in vitro* models of the pulsatile flow.[15,16]. However, the feasibility of using Echo-PIV in routine hospital settings for 2D contrast echocardiography for LV cavity opacification has not been sufficiently clarified. A recent experimental study assessed Echo-PIV accuracy against optical PIV for LV flow visualization and revealed a tendency to underestimate the higher velocity when traditional clinical settings were used (frame rate < 100 Hz).[12,16] We attempted to circumvent some of these limitations by using lower contrast particle density for optimal PIV tracking and using a much higher temporal resolution (frame rate: 129–252 Hz). Moreover, previous works that used Echo-PIV in clinics,[34] or in a validation study,[16] employed different parameters because the frame rates were insufficient for quantitatively evaluating velocities values and parameters were designed merely as a statistical measure of the overall flow pattern. The technique employed here presents, instead, a sufficient acquisition frame rate that allowed evaluating actual fluid-dynamics quantities that were further related with LV muscle mechanics.

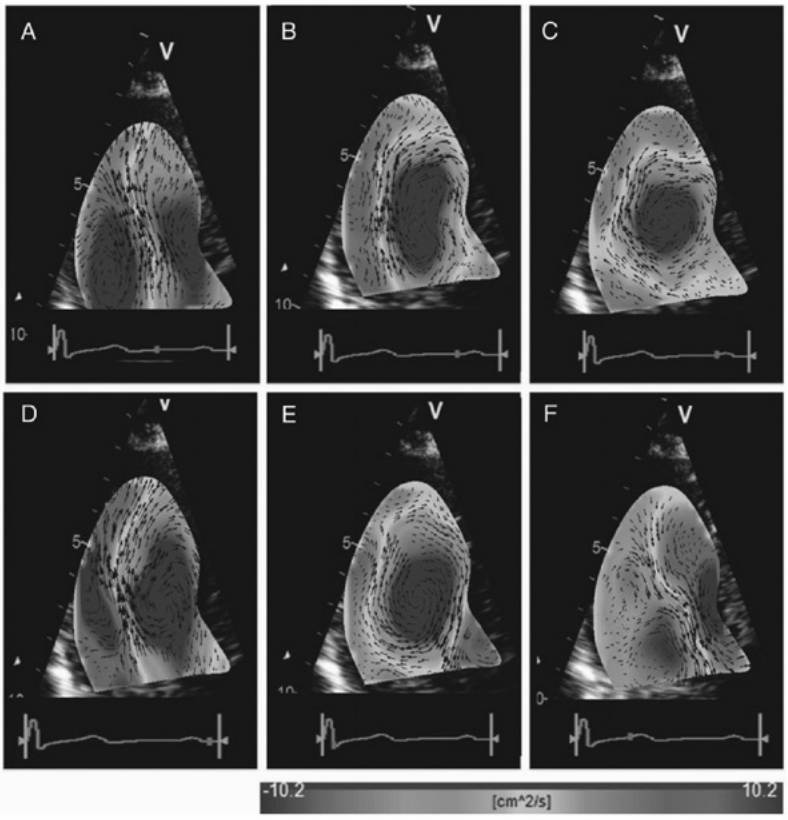

Figure 4. The LV flow sequence during phases of cardiac cycles in a non-HF control subject. LV intracavitary planar vorticity maps of a non-HF control subject (EF 61%) during phases of cardiac cycle are shown in (*A*–*F*). Note that the presence of initial CW (blue) and CCW (red) vortex during early-diastolic filling (*A*). The counterclockiwise flow (red) becomes weaker (*B*) resulting into predominantly CW (blue) vortex during the phase of diastasis (*C*). The atrial flow in late diastole is characterized by an increase in the strength of the CW vortex (*D*), which persists further during IC (*E*). Ejection is characterized by accelerating flow towards the LV outflow surrounded by CW and CCW shear layers (*F*). Movies corresponding to Figure 3 can be viewed as Supplementary data online, *Movies S1* and *S2*.

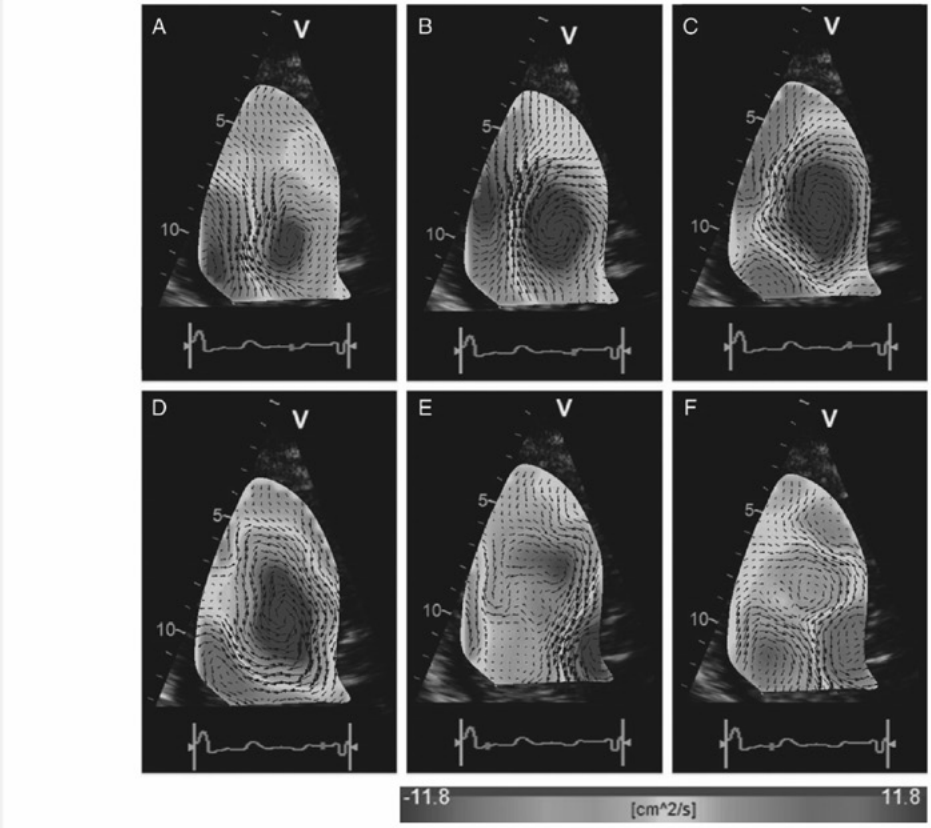

Figure 5. The LV flow sequence in HFREF. LV intracavitary planar vorticity maps of a Stage C HFREF patient (EF 34%) during phases of the cardiac cycle are shown in (*A–F*). The cardiac cycle (*A–F*) is the same as outlined in Figure 3. Note that the CW vortex is attenuated during IC (*E*). Movies corresponding to Figure 4 can be viewed as Supplementary data online, *Movies S3* and *S4*.

Clinical significance

Clinical investigators have recently debated the binary view to HF using the terms systolic and diastolic HF.[42] These data would support the recent suggestions that properties of failing hearts should be considered at different hierarchical scales of performance for understanding the levels of mechanical inefficiencies rather than merely relegating to binary divisions of systolic and diastolic dysfunction.[42] Such integrative analysis of levels of energetic inefficiencies in a failing heart may provide a logical approach to characterizing multidimensional complex interactions between biomarkers in HF syndromes.[43] Although attempts at energetic efficiency of the blood flow were recently measured using the MRI-based assessment of blood flow fields,[44] Echo-PIV is an extension of the LV opacification technique and can be performed in minutes from LV contrast opacification, which is frequently used in HF patients.[45] Another advantage of Echo-PIV is the high-temporal resolution, which permits tracking the blood flow sequence during the transient isovolumic phases of the cardiac cycle. Therefore, the development of echocardiographic techniques for flow visualization has potential for providing a practical technique for characterizing the degree of flow inefficiency in HF patients in clinical practice.

Study limitations

We used apical long-axis views for focusing on the dominant flow structures in the inflow and the outflow regions of the LV. Use of a full 3D structure of flow with incorporation of boundaries would be necessary for more complete assessment of the LV flow structure. The relationships between VS and the ventricle's mechanical performance shown in this investigation also need cautious interpretation. First, the VS alone may not account for other aspects, like the vortex position and its shape with respect to the LV chamber, which may play a role in the flow arrangement and influence LV performance. Furthermore, the formula used for calculating LV

Table 3. Univariate and multivariate linear regression analysis for correlates of VS during IC

	Univariate regression		Multivariate regression				
	Correlation	*P*-value	B	SE	*t*-value	*P*-value	R^2
VS_A (cm^2/s)	0.70	<0.001	0.75	0.10	7.31	<0.001	0.63
VS_E (cm^2/s)	0.57	<0.001					
Ls (%)	−0.34	0.02	−4.44	1.41	−3.14	0.003	
Cs (%)	−0.25	0.10					
Rs (%)	0.28	0.06					
Net twist (degree)	0.30	0.05					

VS_A, vortex strength during late diastole; VS_E, vortex strength during early diastole; Ls, longitudinal strain; Cs, circumferential strain; Rs, radial strain.

Table 4. Clinical and echocardiographic features of HF patients with and without adverse clinical events during follow-up

	Heart failure		*P*-value
	Without events (n = 15)	With events (n = 8)	
Age (years)	71 ± 11	71 ± 9	0.97
Female gender (%)	4 (30)	—	0.30
HFPEF (n) (%)	7 (46)	3 (37)	0.98
Standard echocardiography			
LV septum (mm)	11 ± 2	10 ± 2	0.60
LV end-diastolic dimension (mm)	52 ± 7	58 ± 15	0.27
LV end-systolic dimension (mm)	39 ± 10	50 ± 16	0.12
LVEF (%)	47 ± 16	34 ± 21	0.08
Indexed LA volume (mL/m^2)	46 ± 21	46 ± 8	0.49
E/*A* ratio	1.3 ± 0.5	2.2 ± 1.7	0.14
E/e′ mean	14.7 ± 6.5	24.7 ± 14.0	0.10
RVSP (mmHg)	40 ± 10	44 ± 18	0.75
LV sphericity index	0.66 ± 0.15	0.72 ± 0.15	0.39
LV stroke volume (mL)	65 ± 18	59 ± 21	0.63
LV stroke work (g)	101 ± 31	83 ± 29	0.21
LV mechanical efficiency (mL/s)	61 ± 23	46 ± 22	0.26
Global strains and twist			
Ls (%)	−14.6 ± 4.6	−7.6 ± 5.9	0.002
Cs (%)	−19.0 ± 8.2	−10.9 ± 7.4	0.04
Rs (%)	15.9 ± 9.7	9.0 ± 9.6	0.02
Net twist (degree)	9.5 ± 8.1	5.7 ± 4.3	0.20
Echocardiographic PIV			
VS_E (cm^2/s)	143 ± 67	182 ± 67	0.29
VS_A (cm^2/s)	192 ± 117	155 ± 40	0.54
VS_{IC} (cm^2/s)	219 ± 108	162 ± 32	0.42
VS change	0.24 ± 0.24	−0.08 ± 0.24	0.004

Abbreviations are similar as in *Table 2*.

mechanical efficiency was simplified as the ratio between stroke volume and heart rate. Although this has been shown to provide useful information,[22–25] this theoretical approach differs from previous equations where energy consumption is determined by coronary sinus catheterization to measure real-time myocardial oxygen consumption. Finally, although the difference in VS was associated with adverse cardiac events, the number of events was small and precluded a detailed survival analysis.

Conclusions

The present study establishes the sequence in which LV vortices formed during diastolic filling phases are sustained into IC for the optimal onset of ejection. Our data suggest that the persistence of VS from late diastole into IC is a marker of the fluid-continuum of the cardiac cycle and helps coupling diastole to systole without any intervening periods of haemodynamic stasis. The change in VS is correlated with LV mechanical performance and may have prognostic value for HF patients.

Supplementary data

Supplementary data are available at *European Heart Journal – Cardiovascular Imaging* online.

Funding

This study was supported by an intramural fund (CR-5) from Mayo Clinic, Scottsdale, AZ, USA.

Conflict of interest: none declared.

References

1. Baccani B, Domenichini F, Pedrizzetti G, Tonti G. Fluid dynamics of the left ventricular filling in dilated cardiomyopathy. *J Biomech* 2002;**35**:665–71.
2. Gharib M, Rambod E, Kheradvar A, Sahn DJ, Dabiri JO. Optimal vortex formation as an index of cardiac health. *Proc Natl Acad Sci USA* 2006;**103**:6305–8.
3. Kheradvar A, Gharib M. Influence of ventricular pressure drop on mitral annulus dynamics through the process of vortex ring formation. *Ann Biomed Eng* 2007;**35**: 2050–64.
4. Kheradvar A, Gharib M. On mitral valve dynamics and its connection to early diastolic flow. *Ann Biomed Eng* 2009;**37**:1–13.
5. Pedrizzetti G, Domenichini F. Nature optimizes the swirling flow in the human left ventricle. *Phys Rev Lett* 2005;**95**:108101.
6. Saber NR, Wood NB, Gosman AD, Merrifield RD, Yang GZ, Charrier CL *et al.* Progress towards patient-specific computational flow modeling of the left heart via combination of magnetic resonance imaging with computational fluid dynamics. *Ann Biomed Eng* 2003;**31**:42–52.
7. Subramanian A, Mu H, Kadambi JR, Wernet MP, Brendzel AM, Harasaki H. Particle image velocimetry investigation of intravalvular flow fields of a bileaflet mechanical heart valve in a pulsatile flow. *J Heart Valve Dis* 2000;**9**:721–31.
8. Taylor TW, Yamaguchi T. Flow patterns in three-dimensional left ventricular systolic and diastolic flows determined from computational fluid dynamics. *Biorheology* 1995;**32**:61–71.
9. Carlhall CJ, Bolger A. Passing strange: flow in the failing ventricle. *Circ Heart Fail* 2010;**3**:326–31.
10. Kilner PJ, Yang GZ, Wilkes AJ, Mohiaddin RH, Firmin DN, Yacoub MH. Asymmetric redirection of flow through the heart. *Nature* 2000;**404**:759–61.
11. Sengupta PP, Khandheria BK, Korinek J, Jahangir A, Yoshifuku S, Milosevic I *et al.* Left ventricular isovolumic flow sequence during sinus and paced rhythms: new insights from use of high-resolution Doppler and ultrasonic digital particle imaging velocimetry. *J Am Coll Cardiol* 2007;**49**:899–908.
12. Crapper M, Bruce T, Gouble C. Flow field visualization of sediment-lsaden flow using ultrasonic imaging. *Dyn Atmos Oceans* 2000;**31**:233–45.
13. Kim H, Hertzberg J, Shandas R. Development and validation of echo PIV. *Exp Fluids* 2004;**36**:455–62.
14. Zhang F, Lanning C, Mazzaro L, Barker AJ, Gates PE, Strain WD *et al.* In vitro and preliminary in vivo validation of echo particle image velocimetry in carotid vascular imaging. *Ultrasound Med Biol* 2011;**37**:450–64.
15. Westerdale J, Belohlavek M, McMahon EM, Jiamsripong P, Heys JJ, Milano M. Flow velocity vector fields by ultrasound particle imaging velocimetry: in vitro comparison with optical flow velocimetry. *J Ultrasound Med* 2011;**30**:187–95.
16. Kheradvar A, Houle H, Pedrizzetti G, Tonti G, Belcik T, Ashraf M *et al.* Echocardiographic particle image velocimetry: a novel technique for quantification of left ventricular blood vorticity pattern. *J Am Soc Echocardiogr* 2010;**23**:86–94.
17. Hunt SA, Abraham WT, Chin MH. 2009 Focused Update Incorporated into the ACC/AHA 2005 Guidelines for the Diagnosis and Management of Heart Failure in Adults: a Report of the American College of Cardiology Foundation/ American Heart Association Task Force on Practice Guidelines Developed in Collaboration with the International Society for Heart and Lung Transplantation (vol 53, pg e1, 2009). *J Am Coll Cardiol* 2009;**54**:2464–4.
18. Lang RM, Bierig M, Devereux RB, Flachskampf FA, Foster E, Pellikka PA *et al.* Recommendations for chamber quantification: a report from the American Society of Echocardiography's Guidelines and Standards Committee and the Chamber Quantification Writing Group, developed in conjunction with the European Association of Echocardiography, a branch of the European Society of Cardiology. *J Am Soc Echocardiogr* 2005;**18**:1440–63.
19. Nagueh SF, Appleton CP, Gillebert TC, Marino PN, Oh JK, Smiseth OA *et al.* Recommendations for the evaluation of left ventricular diastolic function by echocardiography. *Eur J Echocardiogr* 2009;**10**:165–93.
20. Yiu SF, Enriquez-Sarano M, Tribouilloy C, Seward JB, Tajik AJ. Determinants of the degree of functional mitral regurgitation in patients with systolic left ventricular dysfunction: a quantitative clinical study. *Circulation* 2000;**102**:1400–6.
21. de Simone G, Devereux RB, Ganau A, Hahn RT, Saba PS, Mureddu GF *et al.* Estimation of left ventricular chamber and stroke volume by limited M-mode echocardiography and validation by two-dimensional and Doppler echocardiography. *Am J Cardiol* 1996;**78**:801–7.
22. de Simone G, Chinali M, Galderisi M, Benincasa M, Girfoglio D, Botta I *et al.* Myocardial mechano-energetic efficiency in hypertensive adults. *J Hypertens* 2009;**27**: 650–5.
23. Schramm W. The units of measurement of the ventricular stroke work: a review study. *J Clin Monit Comput* 2010;**24**:213–7.
24. Cioffi G, Russo TE, Selmi A, Stefenelli C, Furlanello F. Analysis of left ventricular systolic function by midwall mechanics in patients with obstructive sleep apnoea. *Eur J Echocardiogr* 2011;**12**:61–8.
25. Kozakova M, Malshi E, Morizzo C, Pedri S, Santini F, Biolo G *et al.* Impact of prolonged cardiac unloading on left ventricular mass and longitudinal myocardial performance: an experimental bed rest study in humans. *J Hypertens* 2011;**29**: 137–43.
26. Pirat B, Khoury DS, Hartley CJ, Tiller L, Rao L, Schulz DG *et al.* A novel feature-tracking echocardiographic method for the quantitation of regional myocardial function: validation in an animal model of ischemia-reperfusion. *J Am Coll Cardiol* 2008;**51**:651–9.
27. Gao H, Claus P, Amzulescu MS, Stankovic I, D'Hooge J, Voigt JU. How to optimize intracardiac blood flow tracking by echocardiographic particle image velocimetry? Exploring the influence of data acquisition using computer-generated data sets. *Eur Heart J Cardiovasc Imaging* 2012;**13**:490–9.
28. Sengupta PP, Pedrizzetti G, Kilner PJ, Kheradvar A, Ebbers T, Tonti G *et al.* Emerging trends in CV flow visualization. *JACC Cardiovasc Imaging* 2012;**5**:305–16.
29. Kheradvar A, Pedrizzetti G. *Vortex Formation in the Cardiovascular System*. London: Springer-Verlag, 2012.
30. Bland JM, Altman DG. Statistical methods for assessing agreement between two methods of clinical measurement. *Lancet* 1986;**1**:307–10.
31. Kim WY, Walker PG, Pedersen EM, Poulsen JK, Oyre S, Houlind K *et al.* Left ventricular blood flow patterns in normal subjects: a quantitative analysis by three-dimensional magnetic resonance velocity mapping. *J Am Coll Cardiol* 1995;**26**: 224–38.
32. Bolger AF, Heiberg E, Karlsson M, Wigstrom L, Engvall J, Sigfridsson A *et al.* Transit of blood flow through the human left ventricle mapped by cardiovascular magnetic resonance. *J Cardiovasc Magn Reson* 2007;**9**:741–7.
33. Walker PG, Cranney GB, Grimes RY, Delatore J, Rectenwald J, Pohost GM *et al.* Three-dimensional reconstruction of the flow in a human left heart by using magnetic resonance phase velocity encoding. *Ann Biomed Eng* 1996;**24**:139–47.
34. Hong GR, Pedrizzetti G, Tonti G, Li P, Wei Z, Kim JK *et al.* Characterization and quantification of vortex flow in the human left ventricle by contrast echocardiography using vector particle image velocimetry. *JACC Cardiovasc Imaging* 2008;**1**:705–17.
35. Ishizu T, Seo Y, Ishimitsu T, Obara K, Moriyama N, Kawano S *et al.* The wake of a large vortex is associated with intraventricular filling delay in impaired left ventricles with a pseudonormalized transmitral flow pattern. *Echocardiography* 2006; **23**:369–75.
36. Cho EJ, Caracciolo G, Khandheria BK, Steidley DE, Scott R, Abhayaratna WP *et al.* Tissue Doppler image-derived measurements during isovolumic contraction predict exercise capacity in patients with reduced left ventricular ejection fraction. *JACC Cardiovasc Imaging* 2010;**3**:1–9.
37. Rankin JS, McHale PA, Arentzen CE, Ling D, Greenfield JC Jr, Anderson RW. The three-dimensional dynamic geometry of the left ventricle in the conscious dog. *Circ Res* 1976;**39**:304–13.
38. Sengupta PP, Korinek J, Belohlavek M, Narula J, Vannan MA, Jahangir A *et al.* Left ventricular structure and function: basic science for cardiac imaging. *J Am Coll Cardiol* 2006;**48**:1988–2001.
39. Sengupta PP. Exploring left ventricular isovolumic shortening and stretch mechanics: 'The heart has its reasons...'. *JACC Cardiovasc Imaging* 2009;**2**:212–5.

40. Knaapen P, Germans T, Knuuti J, Paulus WJ, Dijkmans PA, Allaart CP *et al.* Myocardial energetics and efficiency: current status of the noninvasive approach. *Circulation* 2007;**115**:918–27.
41. Kim HB, Hertzberg J, Lanning C, Shandas R. Noninvasive measurement of steady and pulsating velocity profiles and shear rates in arteries using echo PIV: in vitro validation studies. *Ann Biomed Eng* 2004;**32**:1067–76.
42. De Keulenaer GW, Brutsaert DL. Systolic and diastolic heart failure are overlapping phenotypes within the heart failure spectrum. *Circulation* 2011;**123**:1996–2004; discussion 2005.
43. Azuaje FJ, Dewey FE, Brutsaert DL, Devaux Y, Ashley EA, Wagner DR. Systems-based approaches to cardiovascular biomarker discovery. *Circ Cardiovasc Genet* 2012;**5**:360–7.
44. Eriksson J, Dyverfeldt P, Engvall J, Bolger AF, Ebbers T, Carlhall CJ. Quantification of presystolic blood flow organization and energetics in the human left ventricle. *Am J Physiol Heart Circ Physiol* 2011;**300**:H2135–41.
45. Kurt M, Shaikh KA, Peterson L, Kurrelmeyer KM, Shah G, Nagueh SF *et al.* Impact of contrast echocardiography on evaluation of ventricular function and clinical management in a large prospective cohort. *J Am Coll Cardiol* 2009;**53**:802–10.

IMAGE FOCUS

doi:10.1093/ehjci/jet095
Online publish-ahead-of-print 18 May 2013

Is it really fat? Ask a T1-map

Vanessa M. Ferreira*, Cameron J. Holloway, Stefan K. Piechnik, Theodoros D. Karamitsos, and Stefan Neubauer

Department of Cardiovascular Medicine, University of Oxford, John Radcliffe Hospital, Oxford, UK

* Corresponding author. Tel: +44 1865221873; fax: +44 1865740449; Email: vanessa.ferreira@cardiov.ox.ac.uk

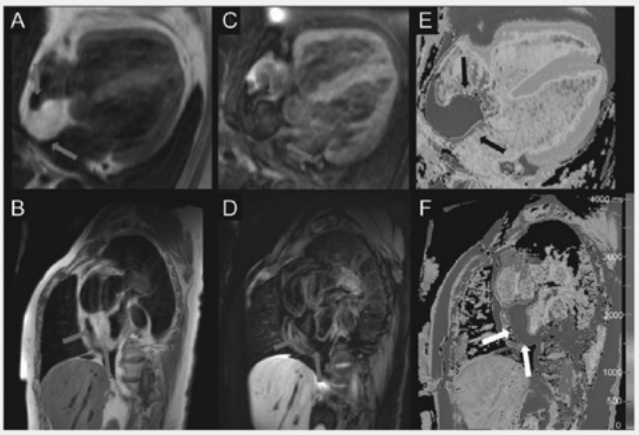

A 67-year-old woman initially presented with dyspnoea. Echocardiography demonstrated an inter-atrial mass. Cardiovascular magnetic resonance (CMR) showed a well-marginated mass (35 mm × 45 mm) in the inter-atrial septum (IAS) sparing the fossa ovalis, extending to the posterior right atrial wall. The mass had high signal intensity on T1-weighted images (*Panels A* and *B*, arrows) consistent with fat, which attenuated on fat-suppression imaging (*Panels C* and *D*, arrows). Native T1-maps (*Panels E* and *F*, arrows) showed homogenous and significantly lower T1 values (230–350 ms) compared with the normal myocardium (green) and blood (yellow/red), but similar to subcutaneous and epicardial fat (blue). The mass had no late gadolinium enhancement and was stable in the size compared with 1-year prior. Findings were consistent with lipomatous hypertrophy of the IAS.

This is a first demonstration of using native T1-mapping for immediate visual and quantitative tissue characterization of an intracardiac mass to help confirm its fat content. T1-maps provide pixel-wise estimates of the T1 relaxation times of the underlying tissue, and each tissue type exhibits a characteristic normal range of T1 values. This allows the visual differentiation of tissues using colour scales as shown. Lipomatous hypertrophy of the IAS is an unencapsulated proliferation of adipose tissue $\geq$20 mm within the atrial septum that is in continuity with epicardial fat. It is associated with older age, increased fat elsewhere in the body, atrial arrhythmias and in some cases, obstruction of the superior vena cava. The correct differentiation of this benign cardiac mass from other atrial tumours using multi-parametric tissue characterization techniques on CMR can prevent unnecessary invasive interventions.

Funding

Funding to pay the Open Access publication charges for this article was provided by the Division of Cardiovascular Medicine, Radcliffe Department of Medicine, University of Oxford.

Circulation Journal
Official Journal of the Japanese Circulation Society
http://www.j-circ.or.jp

ORIGINAL ARTICLE
Heart Failure

Myocardial Stretch in Early Systole is a Key Determinant of the Synchrony of Left Ventricular Mechanical Activity in Vivo

Giuseppe Caracciolo, MD, PhD; Georg Goliasch, MD, PhD; Makoto Amaki, MD, PhD; Manish Bansal, MD; Ayumi Nakabo, MD; Haruhiko Abe, MD; Luis Scott, MD; Luka Lipar, MD; Gianni Pedrizzetti, PhD; Jagat Narula, MD, PhD; Partho P. Sengupta, MD

Background: Recent in-vitro observations suggest that left ventricular (LV) contraction is powered by 'stretch activation', an intrinsic mechanism by which the stretching of an activated cardiomyocyte causes delayed force redevelopment. We hypothesized that mechanical dyssynchrony is related to prolonged early systolic stretch that delays the timing of peak segmental shortening.

Methods and Results: The time intervals from R wave to segmental longitudinal stretch in early systole ($T_{stretch}$) and peak shortening (T_{peak}) and the respective standard deviations ($\sigma T_{stretch}$ and σT_{peak}) were measured by speckle-tracking echocardiography in 57 patients undergoing cardiac resynchronization therapy (CRT). The percentage of time spent in shortening, normalized to T_{peak} duration [corrected $\Delta T=(T_{peak}-T_{stretch})/T_{peak}$] correlated with LV reverse remodeling (reduction in end-systolic volume ≥15%). Of the 57 patients, 40 (70.2%) demonstrated LV reverse remodeling at an average follow-up of 263±125 days after CRT. At baseline, $T_{stretch}$ and $\sigma T_{stretch}$ correlated with T_{peak} and σT_{peak}, respectively. Though there was no difference in $T_{stretch}$, T_{peak}, $\sigma T_{stretch}$ and σT_{peak} between responders and non-responders, corrected ΔT in the mid-lateral and mid-septal segments was shorter in the responders ($P<0.05$ for both) and the average of the 2 independently predicted LV reverse remodeling (area under the curve: 0.77, P=0.001).

Conclusions: Mapping LV segmental shortening in relation to early systolic stretch may aid dyssynchrony assessment in patients undergoing CRT. (*Circ J* 2013; **77:** 2526–2534)

Key Words: Cardiac resynchronization therapy; Heart failure; Left ventricular function

Cardiac resynchronization therapy (CRT) is an important therapeutic option for patients with advanced heart failure (HF).[1] Numerous studies have confirmed the significant improvement in symptoms, increase in exercise capacity and substantial reduction in both death and hospitalization with CRT in appropriately selected patients with systolic HF.[1–4] However, despite careful patient selection, the response rate to CRT ranges only around 60–70%.[2,5,6] Because CRT is an expensive form of therapy and invasive, extensive efforts are being made to improve patient selection and thus, the response rate. A number of echocardiographic parameters have been evaluated for this purpose and have shown promise in the initial studies.[7–9] However, the results from more recent large-scale trials have highlighted the limitations of echocardiographic measures of dyssynchrony and have questioned their accuracy for predicting the therapeutic response of patients undergoing CRT.[10–13]

Recent in-vitro observations suggest that left ventricular (LV) contraction is powered by 'stretch activation', an intrinsic length-sensing mechanism that modulates the contractility of activated cardiomyocytes.[14] Stretching an activated cardiomyocyte causes a delay in timing of force redevelopment by recruitment of additional cross-bridges to force-generating states and helps dynamically adapting the timing of myocardial contraction to the changes in LV preload. In patients with intraventricular conduction abnormalities, the non-uniform electrical activation of the LV myocardium may result in pre-ejection shortening and stretch in segments with

Received September 28, 2012; revised manuscript received April 30, 2013; accepted May 31, 2013; released online July 25, 2013 Time for primary review: 38 days

Division of Cardiovascular Diseases, Mayo Clinic, Scottsdale, AZ (G.C., H.A., L.S., L.L., P.P.S.); Zena and Michael A. Wiener Cardiovascular Institute, Mount Sinai School of Medicine, New York, NY (G.C., G.G., M.A., A.N., H.A., G.P., J.N., P.P.S.), USA; Medanta, The Medicity, Gurgaon (M.B.), India; and Department of Civil Engineering and Architecture, University of Trieste, Trieste (G.P.), Italy

Mailing address: Partho P. Sengupta, MD, FASE, Mount Sinai School of Medicine, 1 Gustave L. Levy Place, PO Box 1030, New York, NY 10029, USA. E-mail: partho.sengupta@mountsinai.org

ISSN-1346-9843 doi:10.1253/circj.CJ-12-1230

premature or late activation, respectively. Such electromechanical dispersion of contractile activity may affect LV function, resulting in global LV dyssynchrony[15] and systolic and diastolic dysfunction.[16] Accordingly, the optimization of electromechanical activity by improving pre-ejection shortening-stretch mechanics may influence global LV performance and explain the benefits of CRT. However, the exact contribution of stretch activation in determining myocardial dyssynchrony and subsequent response to CRT in vivo remains to be proven.

We hypothesized that variability in the mechanical response to CRT is related to non-uniform segmental stretch in early systole, which delays the timing of peak segmental shortening, and sought in this study to develop a specific echocardiographic predictor of CRT response based on this hypothesis.

Methods

This was a retrospective study involving review of clinical history, laboratory data, and echocardiographic findings.

Patient Selection

We identified 68 patients who had undergone CRT at our center on the basis of the recommended clinical criteria: LV ejection fraction ≤35%; QRS >120 ms on ECG, and New York Heart Association symptomatic class III or IV despite optimal medical treatment.[1] Of these, 2 patients did not have a baseline echocardiogram recorded in our data base, 4 patients did not have a post-CRT follow-up and 6 patients had poor echocardiographic image quality and were therefore excluded from the analysis. For the remaining 57 HF patients (74±10 years, 45 men, etiology: 31 nonischemic and 26 ischemic) echocardiographic assessments were performed at baseline, before CRT, and at 263±125 days (101–581 days) after CRT. They were classified as responders to CRT if they displayed a reduction ≥15% in LV end-systolic volume at follow-up, and as non-responders if LV end-systolic volume was reduced by <15%.[17]

Data were collected according to the Mayo Institutional Review Board requirements of those patients who provided informed consent for chart review.

Echocardiographic Assessment

All the patients had a comprehensive 2D and Doppler echocardiogram performed before CRT and after CRT during follow-up. Echocardiographic studies were performed on commercially available ultrasound equipment (Acuson Sequoia, Siemens Medical Solutions USA, Mountain View, CA, USA; Vivid 7, GE Healthcare, Milwaukee, WI, USA) according to the standards recommended by the American Society of Echocardiography.[18] End-diastolic and end-systolic volumes were used to calculate EF by Simpson's biplane method from the apical 4- and 2-chamber views. Pulsed-wave Doppler echocardiography was performed to obtain early (E) and late (A) diastolic transmitral flow velocities and the E/A ratio was calculated. The deceleration time of the mitral E wave was also measured. The pulsed-wave tissue Doppler velocities were measured at the septal and lateral mitral annulus in the 4-chamber view and were averaged for obtaining the mean early diastolic mitral annulus velocity (e') and also the ratio of the early diastolic transmitral flow velocity to the early diastolic mitral annulus velocity (E/e').

Speckle-Tracking Echocardiography (STE)

STE was performed offline on gray-scale images that were obtained at frame rates suitable for the technique (≥30 frames/s) and stored in digital cineloop format (Prosolv Cardiovascular solutions, Indianapolis, IN, USA). The offline analysis was performed using the vendor-customized 2D Cardiac Performance Analysis (2D CPA) software (TomTec Imaging Systems GmbH, Unterschleissheim, Germany) that uses STE technology for the angle-independent measurement of 2D strain. 2D CPA can analyze 2D data from various ultrasound machines and is an extended version of *Syngo*® Velocity Vector Imaging™ (Siemens Medical Solutions USA Inc, Malvern, PA, USA) that has been previously validated with sonomicrometry[19,20] and magnetic resonance imaging.[21,22] 2D CPA, similar to velocity vector imaging, determines myocardial motion from a user-defined tracing along the subendocardial border. Defined endocardial and automated subepicardial borders are traced throughout 1 cardiac cycle by successive application of a series of tracking steps. From this motion, myocardial velocity and strain components are calculated for both endocardial and subepicardial regions along the trace.[23] The apical 4-chamber view was used for deriving subendocardial longitudinal strain (LS) and transverse peak systolic strain from 6 segments in the interventricular septum and lateral wall. The radial strain (RS) and subendocardial circumferential strain (CS) were obtained from 6 segments in the mid-ventricular short-axis view of the LV at the level of the papillary muscles. The peak systolic values for all the different strain parameters were recorded and analyzed. Assessment of the LV strain was regarded as suboptimal when either (1) speckle-tracking could not be obtained for at least 4 of the 6 myocardial segments in the apical 4-chamber or short-axis views; or (2) a visually unacceptable tracking was obtained. From the obtained endocardial LS curves we measured the following: time intervals from the onset of earliest deflection (onset of Q or R wave on the surface ECG) to peak longitudinal stretching in early systole ($T_{stretch}$) (presence of a positive strain before aortic valve closure) and peak shortening (T_{peak}) for each myocardial segment before and after CRT (**Figure 1A**); the proportion of the time spent in shortening (ΔT) was calculated as the difference in the 2 time intervals and was indexed to T_{peak} [corrected $\Delta T = (T_{peak} - T_{stretch})/T_{peak}$]; the segmental values were then averaged to derive the average time intervals and the standard deviations thereof ($\sigma T_{stretch}$ and σT_{peak}). If there no stretch was found, $T_{stretch}$ was zero and ΔT would be 1. Similarly, the presence of a rebound stretch after an initial aborted phase of shortening in any segment was measured as a stretch if the value became positive (**Figure 1**). Cubic spline interpolation was used to normalize segmental LS throughout the cardiac cycle to end-systolic volume (**Figure 1A**). The offline analysis was performed independently by 1 observer who was neither involved in image acquisition nor had knowledge of the other echocardiographic measures of LV function.

Assessment of Echocardiographic Dyssynchrony Indices

Mechanical dyssynchrony indices were assessed to calculate the intraventricular mechanical dyssynchrony. Both radial and circumferential dyssynchrony was assessed from mid-LV short-axis views and defined as the time difference between the anteroseptal and posterior wall segmental peak values.[24] A predefined cut-off value ≥130 ms was considered as significant dyssynchrony.[25,26]

Statistical Analysis

The statistical analysis was performed with commercially available statistics software (MedCalc 11.2, MedCalc Software,

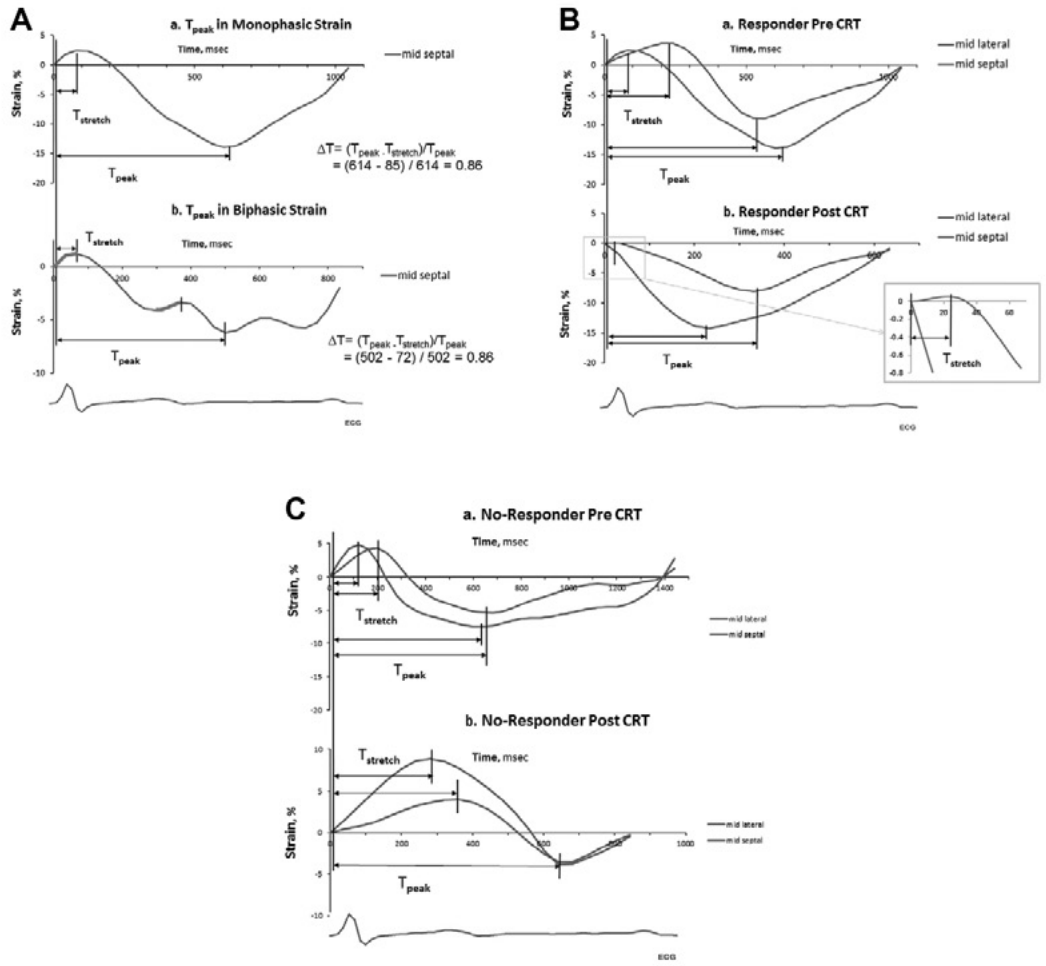

Figure 1. (**A**) Regional systolic stretch measurement, $T_{stretch}$, was measured as the time interval from the peak of R wave on the ECG to the peak stretch during initial systole (**a**) and T_{peak} as the time interval from the peak of R wave to the peak shortening. Presence of a rebound stretch usually seen during ejection often coexisted with the initial stretch (**b**). Rebound septal stretch was measured as $T_{stretch}$ only if the value became positive. (**B**) Regional longitudinal strain curves obtained by speckle-tracking echocardiography in the apical 4-chamber view in a responder patient before (**a**) and after (**b**) cardiac resynchronization therapy (CRT). Corrected ΔT was 0.54 (mid-lateral), 0.87 (mid-septal) before CRT and 0.92 (mid-lateral), 1.0 (mid-septal) after CRT. Note the reduction in $T_{stretch}$ in both the mid-septal and lateral wall segments, although the reduction in stretch is more marked in the lateral wall. (**C**) Regional longitudinal strain curves obtained by speckle-tracking echocardiography in the apical 4-chamber view in a non-responder patient before (**a**) and after (**b**) CRT. Corrected ΔT was 0.71 (mid-lateral), 0.56 (mid-septal) before CRT and 0.56 (mid-lateral), 0.44 (mid-septal) after CRT.

Mariakerke, Belgium). All continuous data are reported as mean±standard deviation and the categorical data as numbers and percentages. The study population was divided into CRT responders and non-responders based on the extent of LV reverse remodeling as described before. Comparisons between 2 groups were made using Student's t-test for normally distributed continuous data and the chi-square test for categorical variables. When the D'Agostino-Pearson test of normality revealed that data did not conform to a normal distribution, a non-parametric test (Kruskal-Wallis test or the Mann-Whitney U test as appropriate) was used. The Wilcoxon test for paired samples was also used to compare the responders group at baseline and after CRT, and the non-responder group at baseline and after CRT. Pearson's correlation was used for assessing the relationship between different timing parameters. Univariate logistic regression analysis was used to assess potential predictors of CRT response, testing various clinical, echocardiographic and strain measurements. Receiver-operating char-

Table 1. Clinical Characteristics of the Study Subjects

	Non-responders (n=17)	Responders (n=40)	P value
Age, years	72±15	76±8	0.68
Female, n	5 (29%)	7 (18%)	0.51
Height, cm	173±12	175±11	0.76
Weight, kg	84±18	86±17	0.87
Body mass index, kg/m^2	28±4	28±5	1.00
Systolic BP, mmHg	116±21	121±18	0.34
Diastolic BP, mmHg	69±13	72±12	0.49
Heart rate, beats/min	71±13	78±17	0.18
QRS pre-CRT, ms	149±35	155±33	0.49
QRS post-CRT, ms	151±25	151±16	0.68
QRS pre > QRS post, n	6 (35%)	24 (60%)	0.15
Left bundle branch block, n	8 (47%)	20 (50%)	0.93
Right bundle branch block, n	–	2 (5%)	–
Right ventricle pacing, n	3 (18%)	6 (15%)	0.70
NYHA class pre-CRT	2.8±0.3	2.4±0.6	0.69
NYHA class post-CRT	2.9±0.4	2.0±0.5	0.99
NYHA class clinical responders, n	11 (65%)	36 (90%)	0.05
Diabetes, n	6 (35%)	7 (18%)	0.26
Hypertension, n	8 (47%)	28 (70%)	0.17
Hyperlipidemia, n	12 (70%)	24 (60%)	0.64
Coronary artery disease, n	12 (70%)	15 (38%)	0.04
MR ≥ moderate pre-CRT, n	3 (18%)	10 (25%)	0.79
MR ≥ moderate post-CRT, n	2 (12%)	3 (8%)	0.99
Renal failure (serum creatinine >1.2 mg/dl), n	4 (24%)	19 (48%)	0.16
Medications			
ACEI or ARB, n	14 (82%)	29 (73%)	0.64
β-blocker, n	14 (82%)	29 (73%)	0.64
Digoxin, n	6 (35%)	10 (25%)	0.63
Diuretics, n	4 (24%)	6 (15%)	0.69

ACEI, angiotensin-converting enzyme inhibitor; ARB, angiotensin receptor blocker; BP, blood pressure; CRT, cardiac resynchronization therapy; MR, mitral regurgitation; NYHA, New York Heart Association.

Table 2. Conventional 2D and Doppler Echocardiographic Parameters of the Study Subjects

	Pre-CRT		Post-CRT	
	Non-responders (n=17)	Responders (n=40)	Non-responders (n=17)	Responders (n=40)
Interventricular septal end-diastolic thickness, mm	11±2	12±3	12±2	12.5±3
Posterior wall end-diastolic thickness, mm	11±2	12±3	11±2	12±2.5
LV end-diastolic dimension, mm	62±7	59±11	61±6	54±10*‡
LV end-systolic dimension, mm	51±7	49±12	51±9	42±11*‡
LV end-diastolic volume, ml	142±46	169±76	179±48†	111±52*‡
LV end-systolic volume, ml	98±36	123±69	127±49†	66±45*‡
LVEF, %	30±10	28±11	33±13†	42±13*‡
Indexed LA volume, ml/m^2	51±24	45±16	56±28	43±23*
E velocity, m/s	0.9±0.3	0.8±0.3	0.9±0.4	0.7±0.3‡
A velocity, m/s	0.6±0.2	0.7±0.3	0.6±0.3	0.7±0.3
E/A ratio	1.6±0.9	1.1±0.7	2.0±1.7	1.1±0.7
Deceleration time, ms	172±42	167±62	207±72	221±59‡
e'mean, m/s	7.4±3	6.5±2.4	6.0±2.3†	6.8±2.6
E/e'mean	14±9	14±7	19±14†	12±5

*P<0.05 vs. post-CRT non-responders; †P<0.05 vs. pre-CRT non-responders; ‡P<0.05 vs. pre-CRT responders.
A, late diastolic mitral inflow velocity; E, early diastolic mitral inflow velocity; e', early diastolic mitral annular velocity; EF, ejection fraction; LA, left atrium; LV left ventricular. Other abbreviation as in Table 1.

Table 3. Speckle-Tracking Echocardiography-Based Strain Parameters of the Study Subjects

	Pre-CRT		Post-CRT	
	Non-responders (n=17)	Responders (n=40)	Non-responders (n=17)	Responders (n=40)
Global strains				
LS endocardial, %	−7.1±5.4	−7.6±4.3	−6.3±4.3	−9.2±5.2
LS transverse, %	6.0±5.7	6.7±5.6	7.6±4.6	8.3±5.7
CS endocardial, %	−8.5±5.4	−8.1±5.4	−8.1±5.6	−11.4±6.4‡
RS, %	6.1±5.7	6.7±5.6	7.6±4.6	9.1±7
Speckle-tracking strain dyssynchrony				
Radial delay ≥130 ms, (%)	10 (59)	19 (50)	9 (53)	18 (47)
Circumferential delay ≥130 ms, (%)	4 (24)	14 (37)	4 (24)	11 (29)
Timing of mechanical events				
Average $T_{stretch}$	90±66	125±66	137±79†	115±83
$6T_{stretch}$	97±60	113±88	98±65	86±51
Average T_{peak}	478±113	492±126	470±104	481±128
$6T_{peak}$	165±111	141±88	135±84	105±56‡
corrected ΔT	0.82±0.11	0.75±0.10*	0.71±0.12†	0.78±0.12
Regional corrected ΔT				
Apical-lateral	0.78±0.20	0.76±0.24	0.78±0.17	0.83±0.18
Mid-lateral	0.84±0.19	0.71±0.19*	0.67±0.27†	0.79±0.17‡
Basal-lateral	0.83±0.17	0.76±0.15	0.75±0.21	0.77±0.17
Apical-septum	0.84±0.20	0.78±0.23	0.76±0.16	0.74±0.21
Mid-septum	0.90±0.15	0.77±0.19*	0.71±0.20†	0.80±0.19
Basal-septum	0.85±0.19	0.80±0.21	0.81±0.17	0.77±0.19

*P<0.05 vs. pre-CRT non-responders; †P<0.05 vs. pre-CRT non-responders; ‡P<0.05 vs. pre-CRT responders. LS, longitudinal strain; CS, circumferential strain; RS, radial strain. Other abbreviation as in Table 1. (Please see text for the details of the timing events.)

acteristic (ROC) curve analysis was performed to determine the optimal cut-off values of different strain measurements for predicting CRT response. P<0.05 was considered statistically significant. Interobserver agreement and intraobserver consistency are presented using interclass correlation coefficients and a 95% confidence interval (95% CI).

Results

Of the 57 patients, 40 (70.2%) demonstrated LV reverse remodeling at an average follow-up of 263±125 days after CRT and were labeled as 'responders', leaving the remaining 17 as 'non-responders'.

Clinical Characteristics

The baseline clinical characteristics of the 57 patients included in the present study are summarized in Table 1. There was no significant difference between the 2 groups with respect to the demographic data, cardiovascular risk factors and medications, with the exception of a higher prevalence of coronary artery disease in the non-responders group (70% vs. 38%, P=0.04). The pre- and post-CRT QRS duration and morphology on ECG were also not different in the 2 groups.

2D and Doppler Echocardiography

Table 2 summarizes the standard 2D and Doppler echocardiographic characteristics of the study group. At baseline, LV end-systolic and end-diastolic dimensions and volumes, and the LV ejection fraction were not significantly different between non-responders and responders. Following CRT, the responders showed a significant reduction in the LV end-systolic and end-diastolic dimensions (42±11 vs. 51±9 mm and 54±10 vs. 61±6 mm, respectively; P<0.01 for both), volumes (66±45 vs. 127±49 ml and 111±52 vs. 179±48 ml, respectively; P<0.01 for both) and a significant increase in the LV ejection fraction (42±13 vs. 33±13 %, P<0.01). In contrast, the LV end-systolic and end-diastolic volumes increased significantly in the non-responders group as compared with baseline (127±49 vs. 98±36 ml and 179±48 vs. 142±46 ml, respectively; P<0.01 for both). In addition, the non-responders showed a reduction in mitral e' and a corresponding increase in mitral E/e' following CRT.

2D Strain Analysis

Table 3 shows the 2D strain parameters, the mechanical dyssynchrony indices and the timing of mechanical events in the 2 groups. At baseline, there was no significant difference in the peak systolic LS, transverse LS, CS and RS for the 2 groups. Radial dyssynchrony index (time difference between time to peak strain between anteroseptum and posterior wall) showed no statistically difference in pre-CRT patients between non-responders and responders. Also, other dyssynchrony indices using circumferential and LS showed no statistical difference between groups.

Following CRT, no significant change was seen in any of the strain parameters in the non-responders. Although LS, transverse LS and RS did not change in the responders either, CS increased significantly in them as compared with baseline (−8.1±5.4 vs. −11.4±6.4%, P=0.01). Mechanical dyssynchrony indices also did not show any significant difference between the groups.

The analysis of timing parameters revealed several interesting findings. In the overall study population, the timing of initial stretch was related to the timing of peak systolic short-

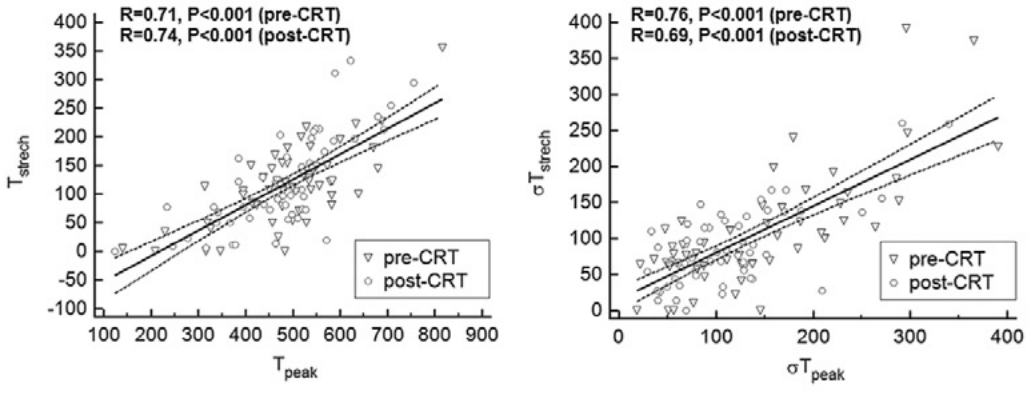

Figure 2. Correlation between the time intervals of the early systolic stretch and the corresponding time intervals of the peak shortening. Please see text for the details.

Table 4. Percentage of Segment in Which the Initial Stretch Was Seen in Non-Responders and Responders

	Non-responder (n=17)	Responder (n=40)	P value
Lateral (any segment)	11 (65%)	36 (90%)	0.05
Basal lateral	9 (53%)	30 (75%)	0.18
Mid-lateral	7 (41%)	30 (75%)	0.27
Apical lateral	10 (59%)	26 (65%)	0.02
Septal (any segment)	12 (71%)	37 (93%)	0.23
Apical septal	7 (41%)	25 (63%)	0.16
Mid-septal	6 (35%)	30 (75%)	0.32
Basal septal	6 (35%)	21 (53%)	0.12

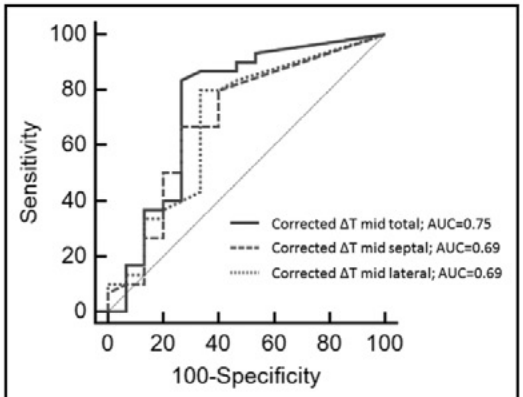

Figure 3. Ability of corrected ΔT, averaged from mid-septum and mid-lateral wall, to predict response to cardiac resynchronization therapy. Please see text for the details. AUC, area under the curve.

ening. This was reflected in the significant correlation seen between the average $T_{stretch}$ and $\sigma T_{stretch}$ and their corresponding shortening parameters when we plotted the relationships for both pre- and post-CRT implantation (Pearson's correlation coefficient 0.71 and 0.74 for average $T_{stretch}$ and T_{peak} and 0.76 and 0.69 for $\sigma T_{stretch}$ and σT_{peak}, P<0.001 for both; **Figure 2**). On comparing the 2 groups, no significant difference was found in the average $T_{stretch}$, T_{peak}, $\sigma T_{stretch}$ and σT_{peak} at baseline. However, the average corrected ΔT was significantly shorter in the responders as compared with the non-responders (0.75±0.10 vs. 0.82±0.11, P=0.03) (**Figure 1B, C**). Following CRT, the corrected ΔT did not change in the responders but shortened significantly in the non-responders (0.71±0.12 from 0.82±0.11, P=0.02). On segmental analysis, compared with non-responders, the responders had significantly shorter corrected ΔT in the mid-septum and mid-lateral wall (0.77±0.19 vs. 0.90±0.15, P=0.01 and 0.71±0.19 vs. 0.84±0.19 respectively, P=0.04; **Figure 1A**). The percentage of segment in which the initial stretch was seen in non-responder and responder patients is shown in **Table 4**. The amount of $T_{stretch}$ was actually longer and ΔT shorter in the lateral wall than in the septum (0.71±0.19 vs. 0.77±0.19; P=0.05) in responders at baseline (**Table 3**). Moreover, ΔT in the lateral wall improved more markedly in responders from baseline to after CRT (0.71±0.19 vs. 0.79±0.17; P=0.02). Similar improvement was not seen in the septal wall in the responders. On ROC curve analysis, the area under the curve (AUC) was higher for averaged baseline ΔT from lateral and septal segments than for mid-lateral and septal segments alone. This is because both lateral and septal segments showed prestretch and CRT reduced prestretch in both the septum and lateral wall (although this was more substantial in the lateral wall), improving ΔT globally after CRT. Baseline ΔT ≤0.82, averaged from the mid-septum and mid-lateral wall, predicted response to CRT (AUC 0.77, P=0.001) independent of lead location and the presence of ischemic cardiomyopathy (**Figure 3**).

For $T_{stretch}$, the intraobserver consistency showed an intraclass correlation of 0.99 with a 95% CI of 0.99–1.00 and the interobserver agreement showed an intraclass correlation of 0.89 with a 95% CI of 0.01–0.99. For corrected ΔT the intraobserver consistency showed an intraclass correlation of 0.98 with a 95% CI of 0.83–0.99 and the interobserver agreement

showed an intraclass correlation of 0.93 with a 95% CI of 0.34–0.99. For T_{peak}, the intraobserver consistency was lower than for $T_{stretch}$ and ΔT and showed an intraclass correlation of 0.74 with a 95% CI of –1.46–0.97. Similarly, the interobserver agreement for T_{peak} was lower than for $T_{stretch}$ and ΔT, with an intraclass correlation of 0.79 with a 95% CI of –1.00–0.97.

Discussion

The present study demonstrates the possible role of myocardial stretch activation in determining the contractile behavior of the LV. To the best of our knowledge, our results show for the first time that early systolic myocardial stretch has a relationship with the timing of peak longitudinal segmental shortening and may be an important determinant of outcome after CRT. Both the lateral wall and septum showed prestretch, which CRT reduced prestretch in both (although it was more substantial in the lateral wall), improving ΔT globally after CRT. This supports previous suggestions that effects of CRT may be related not only to improvement of contractility in late-activated regions, but also to more global effects of uncoordinated activity. Thus CRT improves myocardial shortening and ventricular function in both septal and lateral wall segments in proportion to reductions in abnormal wall stretch, resulting in homogenization of local systolic shortening amplitudes without affecting the total amount of systolic deformation.[27]

In patients with intraventricular conduction defect, dyssynchronous regional contraction of the LV myocardium is considered to play an important role in the development and progression of systolic dysfunction and consequent HF. Accordingly, restoration of the synchronicity of regional LV contraction, by means of CRT, has emerged as a useful therapeutic target in HF patients who remain symptomatic despite optimal medical therapy. A number of studies have shown that in appropriately selected patients with systolic HF, CRT achieves significant reductions in morbidity and mortality and has therefore become the standard-of-care in such patients.[1–4]

Unfortunately, not all patients who receive CRT demonstrate the anticipated hemodynamic and clinical improvements. The available data show that despite strict adherence to the currently accepted selection criteria, the response rate to CRT remains in the range of 60–70% only.[2,5,6] Extensive efforts have been made to define the mechanisms responsible for this variability and to develop tools to help predict the nonresponders. In this context, echocardiographic assessment of mechanical dyssynchrony has received considerable attention. Many Doppler- and non-Doppler-based parameters have been proposed to detect mechanical dyssynchrony and have been shown to predict response to CRT in various studies.[7] However, the PROSPECT (Predictors of Response to Cardiac Resynchronization Therapy) study, which is the most recent, largest, multicenter study to address this issue, failed to show incremental value of any of the echocardiographic measures of dyssynchrony for predicting the response to CRT.[10] Equally disappointing results were seen in other recent, large trials also.[11,28]

Although the mechanisms responsible for the apparent 'failure' of the echocardiographic measures of dyssynchrony continue to be debated, it is noteworthy that all the echocardiographic measures of mechanical dyssynchrony so far have concentrated only on the mid- to late-systolic, ejection phase of the cardiac cycle, with only little or no importance attached to the early systolic events. However, recent in-vitro experiments and animal and human studies have revealed that the overall mechanical performance of the LV is actually determined by the sequences taking place during the early, isovolumic phase of systole.[15,16,29,30]

The LV myocardium has a complex myofiber arrangement characterized by a helical distribution of the layers within the LV wall.[29] This helical arrangement of the myofibers results in simultaneous but opposite movement of the different myocardial regions of the LV, depending largely on the sequence of the electrical activation. Thus, during the isovolumic contraction phase, as the electrical activation wavefront advances from the subendocardial layers to the subepicardial layers, the subendocardial fibers undergo initial shortening whereas the subepicardial fibers are stretched.[30] A similar dispersion of the contractile activity occurs across the entire LV, with the early activated segments undergoing shortening and the late-activated segments getting stretched at the same time. The resultant axial and transmural gradient of the shortening and stretch plays a crucial role in priming the LV for subsequent, effective ejection during the late part of systole.[16] The stretch of the myocytes invokes a 'stretch-activation' mechanism, which is a unique length-sensing mechanism that adjusts the force and timing of the myocyte contraction according to the magnitude of the stretch.[14] This property not only allows the LV to respond to alterations in cardiac load, but is also responsible for the characteristic torsional behavior of the LV.[29] In addition, the sequential activation of the different myocardial regions during early systole helps in accelerating the blood flow axially in the LV apex-to-base direction and from the LV inflow to the LV outflow, which is required for the smooth, energy-efficient ejection of blood. Consequently, the timing of myocardial contraction and relaxation also shows an apex-to-base delay primarily along the long axis of the LV.[29] Therefore, in the present study we focussed on measuring the $T_{stretch}$, T_{peak}, and ΔT primarily along the longitudinal direction of the LV. This coordinated sequence of myocardial stretch and shortening, which is fundamental to the optimum mechanical performance of the LV, was seen to be disrupted in the presence of intraventricular conduction defect and CRT appears to be beneficial through restoration of the normal, synchronized contraction of the LV myocardium.

Although the contribution of the early systolic stretch to LV myocardial mechanics is becoming increasingly recognized, its clinical implications are yet to be proven. To this effect, our study has provided valuable new insights. We found that the duration of the initial stretch was related to the timing of peak shortening, which extends the previous knowledge that early systolic stretch is a determinant of the subsequent contraction. This was further supported by the fact that the percentage of time spent in shortening, instead of the time to peak shortening, was a significant predictor of LV reverse remodeling with CRT. A shorter contraction time, which would mean relatively longer initial stretch, was shown to have greater likelihood of reverse remodeling with CRT. Therefore, our results are consistent with some other data that have been previously shown by other authors.[27] These findings suggest that in patients with intraventricular conduction defect, prolonged, dyssynchronous early systolic stretch of the myocardium adversely affects myocardial contraction and produces a pathophysiological milieu that renders the LV responsive to the beneficial effects of CRT. Interestingly, in the present study, the AUC was higher for averaged baseline ΔT from lateral and septal segments because both the lateral wall and septum showed prestretch that CRT reduced (although it was more substantial in the lateral wall), thus improving ΔT globally after CRT. This sup-

ports previous suggestions that the effects of CRT may be related not only to improvement of contractility in late-activated regions, but also to more global effects of uncoordinated activity. Thus CRT improves myocardial shortening and ventricular function in both the septum and lateral wall in proportion to reductions in abnormal wall stretch, resulting in homogenization of local systolic shortening amplitudes without affecting the total amount of systolic?[27]

Clinical Implications

As mentioned earlier, the lack of adequate therapeutic response in a sizeable proportion of patients has been the Achilles heel of CRT. Despite extensive research, it still remains a major challenge to accurately identify the patients who are unlikely to benefit from the therapy and should therefore be spared this invasive, expensive procedure. Although a number of echocardiographic measures had shown promise in initial studies, the more recent, larger, multicenter trials and a study from Mayo Clinic did not find any of the echocardiographic measures to be accurate enough to reliably predict reverse remodeling with CRT.[10,11] In the present study, learning from the recent insights into myocardial mechanics, we explored a new approach to the echocardiographic assessment of dyssynchrony. Instead of the ejection phase events alone, we assessed the value of early systolic stretch in predicting reverse remodeling following CRT and found encouraging results. In our study, the averaged corrected ΔT had an AUC of 0.77 on ROC analysis, which is significantly higher than the values reported for the other measures in the previous studies.[10,11] These results, if confirmed in further, larger studies, would enable us to identify, with reasonable accuracy, the advanced HF patients who could specifically benefit from CRT.

Study Limitations

Given the retrospective design, the present study had several limitations that merit attention. Most importantly, we were limited by the echocardiographic information that was available for analysis. For example, we could not adequately assess the incremental value of early systolic stretch, over the conventional echocardiographic measures of mechanical dyssynchrony, in determining the response to CRT. However, relatively newer measures of intraventricular dyssynchrony based on longitudinal and RS were measured in the present study and the ΔT was found to predict the CRT response independent of these indices.[25] Similarly, we could measure LS only in the apical 4-chamber view. However, this too was unlikely to have appreciably influenced our findings. Previous studies have consistently shown septum-lateral wall delay on tissue velocity imaging to be one of the most accurate echocardiographic predictors of CRT response.[7] In our study also, the timing of shortening and stretch of the septum and lateral wall were found to have the greatest accuracy for predicting reverse remodeling with CRT. A previous report had shown that scarred segments in the LV have an effect on the assessment of dyssynchrony. This study did not take into consideration the presence of any scarred segments. Finally, mechanical dyssynchrony is only one of several determinants of therapeutic response to CRT. Extent and location of scar, QRS morphology, lead position etc. can all influence the outcome after CRT. Unfortunately, because of the retrospective design and the small sample size, we were unable to study the role of these parameters in determining the response to CRT. Therefore, larger, prospective, multicenter studies with longer follow-up are required to address these issues.

Conclusions

Early systolic myocardial stretch shows a relationship with the timing of peak longitudinal segmental shortening and correlates with the synchrony of LV mechanical performance. Our observations suggest a key role of early systolic stretch in determining the overall mechanical performance of the LV. Mapping LV segmental shortening in relation to the early systolic stretch may aid dyssynchrony assessment and predicting response to CRT.

Disclosures

There is no relationship with industry.

References

1. Jessup M, Abraham WT, Casey DE, Feldman AM, Francis GS, Ganiats TG, et al. 2009 focused update: ACCF/AHA Guidelines for the Diagnosis and Management of Heart Failure in Adults: A report of the American College of Cardiology Foundation/American Heart Association Task Force on Practice Guidelines: Developed in collaboration with the International Society for Heart and Lung Transplantation. *Circulation* 2009; **119:** 1977–2016.
2. Abraham WT, Fisher WG, Smith AL, Delurgio DB, Leon AR, Loh E, et al. Cardiac resynchronization in chronic heart failure. *N Engl J Med* 2002; **346:** 1845–1853.
3. Bristow MR, Saxon LA, Boehmer J, Krueger S, Kass DA, De Marco T, et al. Cardiac-resynchronization therapy with or without an implantable defibrillator in advanced chronic heart failure. *N Engl J Med* 2004; **350:** 2140–2150.
4. Cleland JG, Daubert JC, Erdmann E, Freemantle N, Gras D, Kappenberger L, et al. The effect of cardiac resynchronization on morbidity and mortality in heart failure. *N Engl J Med* 2005; **352:** 1539–1549.
5. Hawkins NM, Petrie MC, MacDonald MR, Hogg KJ, McMurray JJ. Selecting patients for cardiac resynchronization therapy: Electrical or mechanical dyssynchrony? *Eur Heart J* 2006; **27:** 1270–1281.
6. Young JB, Abraham WT, Smith AL, Leon AR, Lieberman R, Wilkoff B, et al. Combined cardiac resynchronization and implantable cardioversion defibrillation in advanced chronic heart failure: The MIRACLE ICD Trial. *JAMA* 2003; **289:** 2685–2694.
7. Gorcsan J 3rd, Abraham T, Agler DA, Bax JJ, Derumeaux G, Grimm RA, et al. Echocardiography for cardiac resynchronization therapy: Recommendations for performance and reporting--a report from the American Society of Echocardiography Dyssynchrony Writing Group endorsed by the Heart Rhythm Society. *J Am Soc Echocardiogr* 2008; **21:** 191–213.
8. Iwano H, Yamada S, Watanabe M, Mitsuyama H, Nishino H, Yokoyama S, et al. Novel strain rate index of contractility loss caused by mechanical dyssynchrony: A predictor of response to cardiac resynchronization therapy. *Circ J* 2011; **75:** 2167–2175.
9. Sakamaki F, Seo Y, Ishizu T, Yanaka S, Atsumi A, Yamamoto M, et al. Tissue Doppler imaging dyssynchrony parameter derived from the myocardial active wall motion improves prediction of responders for cardiac resynchronization therapy. *Circ J* 2012; **76:** 689–697.
10. Chung ES, Leon AR, Tavazzi L, Sun JP, Nihoyannopoulos P, Merlino J, et al. Results of the Predictors of Response to CRT (PROSPECT) trial. *Circulation* 2008; **117:** 2608–2616.
11. Miyazaki C, Redfield MM, Powell BD, Lin GM, Herges RM, Hodge DO, et al. Dyssynchrony indices to predict response to cardiac resynchronization therapy: A comprehensive prospective single-center study. *Circ Heart Fail* 2010; **3:** 565–573.
12. Auricchio A, Prinzen FW. Non-responders to cardiac resynchronization therapy: The magnitude of the problem and the issues. *Circ J* 2011; **75:** 521–527.
13. Seo Y, Ito H, Nakatani S, Takami M, Naito S, Shiga T, et al. The role of echocardiography in predicting responders to cardiac resynchronization therapy. *Circ J* 2011; **75:** 1156–1163.
14. Campbell KB, Chandra M. Functions of stretch activation in heart muscle. *J Gen Physiol* 2006; **127:** 89–94.
15. Coppola BA, Covell JW, McCulloch AD, Omens JH. Asynchrony of ventricular activation affects magnitude and timing of fiber stretch in late-activated regions of the canine heart. *Am J Physiol Heart Circ Physiol* 2007; **293:** H754–H761.
16. Sengupta PP. Exploring left ventricular isovolumic shortening and stretch mechanics: "The heart has its reasons." *JACC Cardiovasc Imaging* 2009; **2:** 212–215.

17. Stellbrink C, Breithardt OA, Franke A, Sack S, Bakker P, Auricchio A, et al. Impact of cardiac resynchronization therapy using hemodynamically optimized pacing on left ventricular remodeling in patients with congestive heart failure and ventricular conduction disturbances. *J Am Coll Cardiol* 2001; **38:** 1957–1965.
18. Lang RM, Bierig M, Devereux RB, Flachskampf FA, Foster E, Pellikka PA, et al. Recommendations for chamber quantification: A report from the American Society of Echocardiography's Guidelines and Standards Committee and the Chamber Quantification Writing Group, developed in conjunction with the European Association of Echocardiography, a branch of the European Society of Cardiology. *J Am Soc Echocardiogr* 2005; **18:** 1440–1463.
19. Korinek J, Wang J, Sengupta PP, Miyazaki C, Kjaergaard J, McMahon E, et al. Two-dimensional strain: A Doppler-independent ultrasound method for quantitation of regional deformation: Validation in vitro and in vivo. *J Am Soc Echocardiogr* 2005; **18:** 1247–1253.
20. Korinek J, Kjaergaard J, Sengupta PP, Yoshifuku S, McMahon EM, Cha SS, et al. High spatial resolution speckle tracking improves accuracy of 2-dimensional strain measurements: An update on a new method in functional echocardiography. *J Am Soc Echocardiogr* 2007; **20:** 165–170.
21. Cho GY, Chan J, Leano R, Strudwick M, Marwick TH. Comparison of two-dimensional speckle and tissue velocity based strain and validation with harmonic phase magnetic resonance imaging. *Am J Cardiol* 2006; **97:** 1661–1666.
22. Li Y, Garson CD, Xu Y, Beyers RJ, Epstein FH, French BA, et al. Quantification and MRI validation of regional contractile dysfunction in mice post myocardial infarction using high resolution ultrasound. *Ultrasound Med Biol* 2007; **33:** 894–904.
23. Geyer H, Caracciolo G, Abe H, Wilansky S, Carerj S, Gentile F, et al. Assessment of myocardial mechanics using speckle tracking echocardiography: Fundamentals and clinical applications. *J Am Soc Echocardiogr* 2010; **23:** 351–369; quiz 453–455.
24. Tanaka H, Nesser HJ, Buck T, Oyenuga O, Janosi RA, Winter S, et al. Dyssynchrony by speckle-tracking echocardiography and response to cardiac resynchronization therapy: Results of the Speckle Tracking and Resynchronization (STAR) study. *Eur Heart J* 2010; **31:** 1690–1700.
25. Suffoletto MS, Dohi K, Cannesson M, Saba S, Gorcsan J 3rd. Novel speckle-tracking radial strain from routine black-and-white echocardiographic images to quantify dyssynchrony and predict response to cardiac resynchronization therapy. *Circulation* 2006; **113:** 960–968.
26. Delgado V, Ypenburg C, van Bommel RJ, Tops LF, Mollema SA, Marsan NA, et al. Assessment of left ventricular dyssynchrony by speckle tracking strain imaging comparison between longitudinal, circumferential, and radial strain in cardiac resynchronization therapy. *J Am Coll Cardiol* 2008; **51:** 1944–1952.
27. Lim P, Donal E, Lafitte S, Derumeaux G, Habib G, Reant P, et al. Multicentre study using strain delay index for predicting response to cardiac resynchronization therapy (MUSIC) study. *Eur J Heart Fail* 2011; **13:** 984–991.
28. Ishikawa T. Limitations and problems of assessment of mechanical dyssynchrony in determining cardiac resynchronization therapy indication. Is assessment of mechanical dyssynchrony necessary in determining CRT indication? (Con). *Circ J* 2011; **75:** 465–471.
29. Sengupta PP, Korinek J, Belohlavek M, Narula J, Vannan MA, Jahangir A, et al. Left ventricular structure and function: Basic science for cardiac imaging. *J Am Coll Cardiol* 2006; **48:** 1988–2001.
30. Ashikaga H, van der Spoel TI, Coppola BA, Omens JH. Transmural myocardial mechanics during isovolumic contraction. *JACC Cardiovasc Imaging* 2009; **2:** 202–211.